J Mater Sci (2019) 54:36–61

Review

Aligned-graphene composites: a review

Fei Wang[1], Haoyu Wang[2], and Jian Mao[1,*]

[1] College of Materials Science and Engineering, Sichuan University, Chengdu 610065, China
[2] School of Materials Science and Engineering, University of New South Wales, Sydney, NSW 2052, Australia

Received: 6 May 2018
Accepted: 21 August 2018
Published online: 1 October 2018

ABSTRACT

Graphene and its derivatives (G) are promising nanofillers with the ability to boost versatile properties of composites despite the low addition due to their combined excellent performances. Moreover, aligning G into various matrices can achieve stronger improvement in properties compared to composites with randomly distributed G. Aligning G is an effective strategy to take full advantage of its properties. In the present work, the state-of-the-art progress in preparations and resulted properties of aligned-graphene (and aligned-graphene derivatives) composites (AGCs) is comprehensively reviewed. The mechanisms of various preparation methods are presented, such as liquid crystal method, vacuum filtration method, and combinations of vacuum filtration and spark plasma sintering method, for both polymer-based and metal-based AGCs. Furthermore, the relevant influencing factors in procedures are analyzed. In addition, influences of aligned-graphene (and aligned-graphene derivatives) on the resulting electric, thermal, and mechanical properties have been discussed and the reasons why AGCs possessed better properties have been summarized. Current challenges associated with AGCs and the pathways toward future progress in AGCs are discussed.

Abbreviations

G	Graphene and its derivatives
GO	Graphene oxide
FLG	Functional graphene
CNTs	Carbon nanotubes
TTD	Through-thickness direction of graphene (graphene derivatives)
EMI	Electromagnetic interference
LC	Liquid crystal method
LBL	Layer-by-layer self-assemble method
UFC	Unidirectional freeze-casting method
VFSPS	Vacuum filtration and spark plasma sintering method
GAD	Graphene (graphene derivative) aqueous dispersions
AG	Aligned-graphene (aligned-graphene derivatives)
TEM	Transmission electron microscope
EP	Epoxy

Address correspondence to E-mail: maojian@scu.edu.cn

https://doi.org/10.1007/s10853-018-2849-4

PAA	Poly(amic acid)
EMF	Exerting magnetic field method
G-Fe_3O_4	Fe_3O_4 anchored graphene (graphene derivatives)
DC	Direct current
1D	One dimensional
G-diamine	Diamine-modified graphene
PDDA	Poly(diallyldiamine chloride)
AGLCs	Aligned-graphene (aligned-graphene derivative) laminated composites
CTAB	Hexadecyl trimethyl ammonium bromide
SLS	Sodium lignosulfonate
GA	Graphene (graphene derivative) aerogel
FETs	Field effect transistors
SPS	Spark plasma sintering
CVDS	Growing graphene by chemical vapor deposition onto surface of metals and sintering the graphene/metals sheets
α	Specific area
RG	Random-graphene (random-graphene derivatives)
PAMPs	Poly(2-acrylamido-2-methyl-1-propanesulfonic acid)
KH550-G	KH550-modified graphene
PI	Polyimide
PEM/PSS/PAH	Polyelectrolyte/poly(sodium 4-styrenesulfonate)/poly(allylamine hydrochloride)
PS-GO	Polystyrene-grafted graphene oxide
SSBR-BR	Solution styrene butadiene/butadiene rubber
λ	Thermal conductivity
EIS	Electrochemical impedance spectroscopy
CA	Cellulose acetate
2D	Two dimensional
rGO	Reduced graphene oxide
TIM	Thermal interface materials
IPD	In-plane direction of graphene (graphene derivatives)
AGCs	Aligned-graphene (aligned-graphene derivative) composites
RGCs	Random-graphene (random-graphene derivative) composites
VF	Vacuum filtration method
SEI	Solvent evaporation induction method
RPS	Replication of the ordered porous structure method
LMPG	Liquid mixtures of polymers and graphene (graphene derivatives)
PTFE	Polytetrafluoroethylene
SEM	Scanning electron microscope
GCA	Graphene carboxylic acid
PU	Polyurethane
PVDF-HFP	Poly(vinylidene fluoride-co-hexafluoropropylene)
EEF	Exerting electric field method
3D	Three dimensional
AC	Alternating current
PVA	Poly vinyl alcohol
MG	Multilayer G
PSS	Poly(styrene sulfonate)
MGACs	Monolithic aligned-graphene (aligned-graphene derivative) composites
SDS	Sodium dodecyl sulfate
PET	Polybutylene terephthalate
SBR	Styrene butadiene rubber
PECVD	Plasma-enhanced chemical vapor deposition
CVD	Chemical vapor deposition
Pc	Percolation threshold value
rGO-Fe_3O_4	Fe_3O_4 anchored reduced graphene oxide
UHMWPE	Ultra-high molecular weight polyethylene
PEEK	Poly(ether ether ketone)
PEDOT	Poly(3,4-ethylene dioxythipphene)
PSI-GO	Poly(styrene-co-isoprene)-grafted graphene oxide
BTESPT	Bis(triethoxysilylpropyl)tetrasulfide
VTMS-GO	Vinyl tri-methoxysilane grated graphene oxide
FGS	Fluorinated graphene
σ	Electronic conductivity

Introduction

G) are allotropes of carbon materials with a 2D structure, which have a unique combination of properties such as excellent tribological property, large α (2600 m^2/g), high electronic conductive property, extraordinary thermal conductivity, and superior mechanical property [1–5]. These properties

suggest the outstanding versatility of G in fillers such as GO, rGO, and FLG for various applications of composites ranging from TIM, structure materials, anti-wear materials, electric conductive materials, and anti-corrosion materials [6–10]. The integration of G is an effective way to boost the performance of composites; however, in many cases, the actual performances of the resulting composites are noticeably lower than the theoretical predictions [11, 12].

The properties intensely respond to the architectures of composites. Therefore, the structural design of composites is a key factor for the improvement of various properties. Research on aligning anisotropic nanofillers (such as the arrangement of nanoscale zinc oxide [11], CNTs [12] and nanofibers [13]) in diverse matrices, thus enabling approximation of the properties of the composites toward the theoretical value, has drawn significant attention and has achieved notable progress in recent years. For example, G is used as an anisotropic 2D material whose properties at IPD are predominantly higher than those of TTD, and it has recently been verified that the orientation control of the distribution of G in matrices can facilitate the resultant properties, thus closing the gap to the theoretical value [14].

In this review, efforts have been devoted to summarizing the fabrications and properties as well as the applications of AGCs. A number of synthetic methods for AGCs have been reviewed, such as the liquid crystal method, the exerting electronic field method, and the exerting magnetic field method. The electrical, thermal, mechanical, anti-corrosion, tribological, and EMI shielding properties of AGCs are mainly discussed, and the reasons for the better performances of AGCs compared to RGCs are analyzed. This review provides guidance and stimulates the development for high-performance AGCs.

Preparations of AGCs

In recent years, a number of methods have been developed for the preparations of various matrices AGCs. The methods reported herein for the preparations of polymer-based AGCs can be divided into six categories: (1) LC, (2) exerting eternal field method (both magnetic field and electronic field), (3) VF, (4) LBL, (5) SEI, and (6) UFC. For metal-based AGCs, there are mainly two ways: (1) RPS and (2) VFSPS. The following provides a detailed discussion of those methods and their influencing factors.

Preparations of polymer-based AGCs

LC

Several of the materials after melting or dissolving, despite the loss of rigidity of solid materials, have obtained liquid flowability, retained the anisotropic orderly crystalline material, and formed an intermediate state with both crystal and liquid properties. The ordered fluid in the process of solid–liquid transformation is called liquid crystal. LC is widely applied to prepare AGCs due to its simplicity. In theory, the G crystalline liquid mainly originates from the ultra-high α and moderate viscosity of the mixtures [15]. Specifically, steric hindrance forms in LMPG and GAD with low viscosity when the flaky G overlaps, and the effect induces a transition from isotropy to a long-range-order liquid crystal structure. In general, researchers use the concentration of G to control the viscosity of mixtures due to the linear relationship between viscosity and concentration. The G critical concentration, which is the lowest concentration for the formation of a liquid crystal, is a central parameter to control the formation of liquid crystal [16]. Aboutalebi et al. quantitatively calculated the G critical concentration by assuming circular G sheets [17]. The G critical concentration can be calculated by Eq. (1):

$$\rho D^3 = \frac{CD^2}{\frac{\pi}{4}td} \tag{1}$$

where D, ρ, C, d, and t represent G diameter, quantity of G of per unit area, concentration of G (in g/m^3), mass density of G (in g/cm), and thickness of G, respectively. Theoretical analysis shows that the liquid crystal phenomenon emerges when the ρD^3 exceeds the critical value of 4.12. As we can see from Eq. (1), the higher α, the easier the liquid crystal can be formed. Figure 1 shows the optical images of the crystal liquid phase with different GO concentrations in water. With increasing GO concentrations, the GO liquid crystal increases. However, exorbitant concentration is not encouraged because high viscosity hampers G spontaneous stacking. Furthermore, the shape of G, the presence of functional groups attached on G, and the viscosity of solvents also

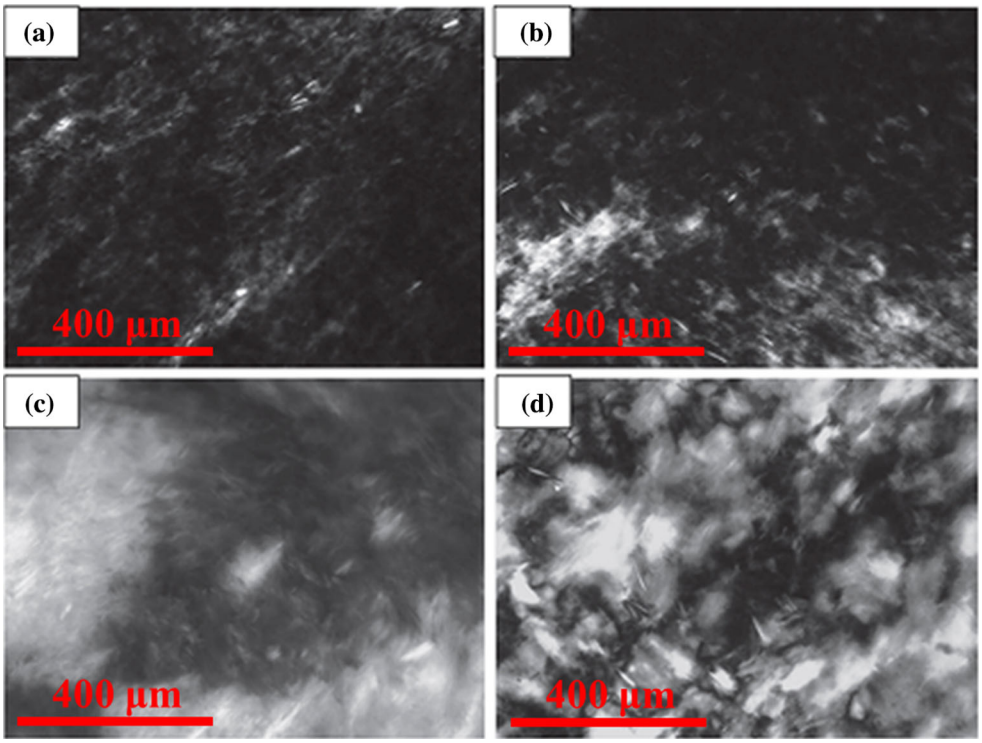

Figure 1 Optical images of liquid crystals with **a** 0.15 wt%, **b** 0.2 wt%, **c** 0.5 wt%, and **d** 1.0 wt% GO in water. (see Ref. [17]).

influence the formation of the liquid crystal, because these factors can affect the steric hindrance behavior.

Following the liquid crystal formation in diverse systems, LMPG curing is conducted by adding curing agents [18], casting [19], and other methods. For instance, a GO liquid crystal formed in chitosan solution at an incorporation of GO above 0.25 wt%; then, the mixtures were casted in molds to obtain AG/chitosan composites [19]. In general, despite the simple procedures of LC, several limitations still exist. (1) Although the macroscopic arrangement of G is perfect (Fig. 2b), the microcosmic distribution of G in matrices is inhomogeneous (Fig. 2d); (2) several parameters, especially the G concentration, are limited at a related narrow range, due to the requirements of critical concentration and viscosity of LMPG.

We summarize the critical concentrations of multifold G forming liquid crystal in diverse systems (in Table 1). In the available reports, the lowest critical concentration (0.1 wt%) of GO was obtained in water [17], due to the small viscosity of the water medium and the large size of GO.

EMF and EEF

G is featured as having diamagnetism, a ubiquitous property of materials due to the magnetic response of orbital electrons [27]. This property enables researchers to align G via the theory of Landau diamagnetism [28]; however, relevant studies are still rare because of the requirement of exerting an enormous magnetic field to rotate G. It is an imperfect technique that cannot be applied and engineered at a large scale. To date, anchoring paramagnetic nanoparticles, especially Fe_3O_4, onto the surface of G is a prevalent practical way to align G under a relatively small external magnetic field.

The EMF (here, the magnetic field is defined as static magnetic field) normally consists of two steps for the preparation of AGCs. The first procedure mainly anchors paramagnetic nanoparticles onto G, then dispersing the magnetic G in liquid polymer solutions to obtain LMPG. Next, the LMPG undergoes curing under the external magnetic field. A schematic of EMF is shown in Fig. 3. The initial G-Fe_3O_4 would rotate parallel to the orientation of the magnetic induction line. One advantage of the strategy is that is imposes few limitations of G concentration and LMPG viscosity, for which it can be

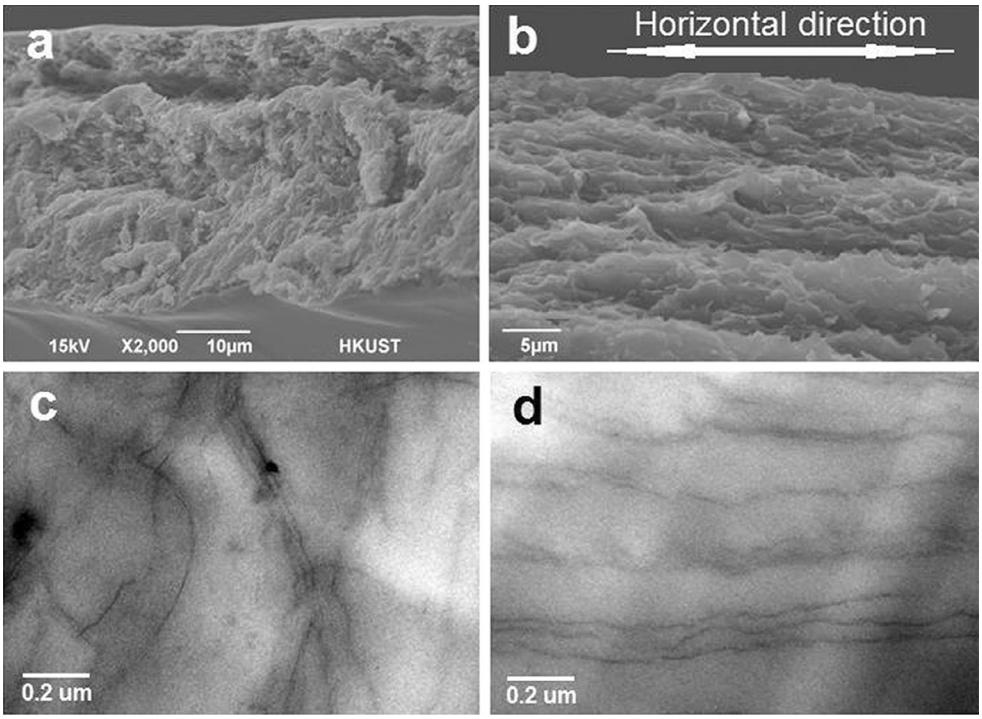

Figure 2 SEM and TEM images of **a**, **c** RGCs and **b**, **d** AGCs.

Table 1 Critical concentration of reported G crystalline liquids

Type of G	Size of G	Medium	G critical concentration	References
GO	~32.70 μm	Water	0.1 wt%	[17]
GO	~2 μm	Waterborne latex of EP	0.12 vol%	[18]
GO	–	Chitosan solution	0.25 wt%	[19]
GO	~32.7 ± 24.3 μm	Emulsion of PU	2 wt%	[20]
rGO	~2 μm	Waterborne latex of PU	0.4 wt%	[21]
GO	~10 μm	Emulsions of PU	2 wt%	[22]
GO	–	PU solution	2 wt%	[23]
GCA	–	PAA solutions	0.4 wt%	[24]
rGO	~10 μm	PVDF-HFP	4.2 wt%	[25]
G	~400 nm	Water	20–30 mg/mL	[26]

potentially applied for preparations of AGCs with ultra-low and ultra-high G contents. A further method allows very convenient control of the alignment direction of G by regulating the orientation of the magnetic induction line. Moreover, it is preferable for G to load nanoparticles than other anisotropic materials, such as CNTs [30] and Al_2O_3 [31], due to their ultrahigh α. EMF can not only be used for the preparation of 2D film materials but is also suitable for the synthesis of 3D bulk materials. Typically, G-Fe_3O_4 hybrid nanoparticles were in situ grown onto G by a coprecipitation method, and the AG/bismaleimides composite was prepared by casting under a 2.0 T external magnetic field [32]. The resultant composites showed excellent tribological properties (friction coefficient as low as 0.07 when the addition of G-Fe_3O_4 content was 0.6 wt%). In another case, Yan et al. deposited Fe_3O_4 (about 8 nm) onto G by a modified coprecipitation method, and the liquid mixture of G-Fe_3O_4 and EP monomer was placed to a 300 mT magnetic field [33]. Finally, AG/EP was obtained by adding a curing agent. The AG/EP composites exhibited obvious anisotropy in thermal conductivity. The increase in thermal conductivity along with IPD was far higher than that in vertical direction. Renteria et al. applied EMF to prepare AG/

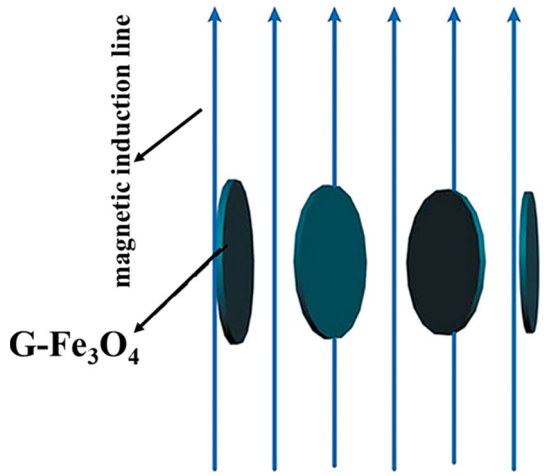

Figure 3 Mechanism of aligning G-Fe_3O_4 by the statics magnetic field. (see Ref. [29]).

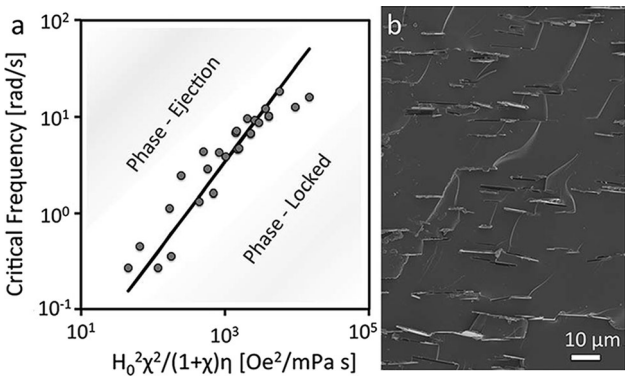

Figure 4 **a** Universal curve shows the dependence of the critical frequency on magnetic field strength, magnetic susceptibility, and fluid viscosity. **b** The cross-section morphology of biaxial alumina platelet composites. (in Ref. [38]).

EP TIM, which led to a decreasing temperature rise by as much as 10 °C in response to the addition of 1 wt% AG in AG direction [34]. In addition to the mentioned applications, the AGCs prepared by EMF were applied in magnetic-controlled switches [35], transparent and flexible electrodes [36], and thermal conductive materials [37].

In recent years, nonlinear alignment dynamics have been demonstrated as a strategy for arraying magnetic nanosheets in suspensions at a biaxial orientation under a rotating magnetic field (Fig. 4b) [38, 39]. The composites possess higher anisotropic properties than those prepared by EMF. The rigorous demands for the strategy shown in Fig. 4a, such as the frequency of the magnetic field and the rheological properties of the LMPG, require research into the alignment of G by rotating magnetic field; however, no such studies have been published to date.

Nanoparticles with high electron mobility are easily polarized and generate orientation torsion under the induction of an electric field, followed by alignment along the direction of parallel to electric field [40]. The essential metrics of G and rGO, high electron mobility, and large α, are available for preparing AGCs by EEF. Both DC or AC can achieve the alignment of G in liquid; however, G is inclined to electrophoretic alignment in DC electric field resulting in their aggregation near electrodes [41]. Therefore, AC is often used to induce G orientation. Wang presented an analytical model to predict the electric field-induced alignment of cantilevered G nanoribbons and showed that G can be easily arrayed than CNTs under electric fields [42]. Experimentally, AG/EP composites were prepared by exerting an AC electric field (25 V/mm, 10 kHz), and the as-prepared composites exhibited 7–8 orders of magnitude improvement in the electrical conductivity and achieve an increase in the mode I fracture toughness of nearly 900% [41]. Pang et al. prepared AG/polystyrene composites by EEF in the process of annealing and verified that G formed the conductive network easier than CNTs [43]. Compared to EMF, EEF is a relatively rare technique for preparing AGCs, because the high experimental equipment and energy consumption requirements restrict its large-scale development and application.

VF

G and CNTs inherit the major feature of 2D and 1D structures, respectively, which equip them with facile fabrication of anisotropic stacked structure by the flowing of solvents [44, 45]. For G, the VF is not only suitable for the preparation of 2D AG membrane composites, but is also available for preparing 3D bulk AGCs. VF consists of two approaches shown in Fig. 5. Approach (i) obtains G paper by filtrating GAD and then penetrating aimed polymers monomers into G layers of G paper by soaking the G paper in the polymer monomer liquid. Finally, ACGs are obtained by polymer monomer polymerization. Typically, G was dispersed in a mixture of water and ethanol (at a volume ratio of 1:4), and then, the mixture was vacuum-filtrated with a PTFE membrane to obtain the G paper. Next, the G paper was immersed in a mixture of EP monomer and curing

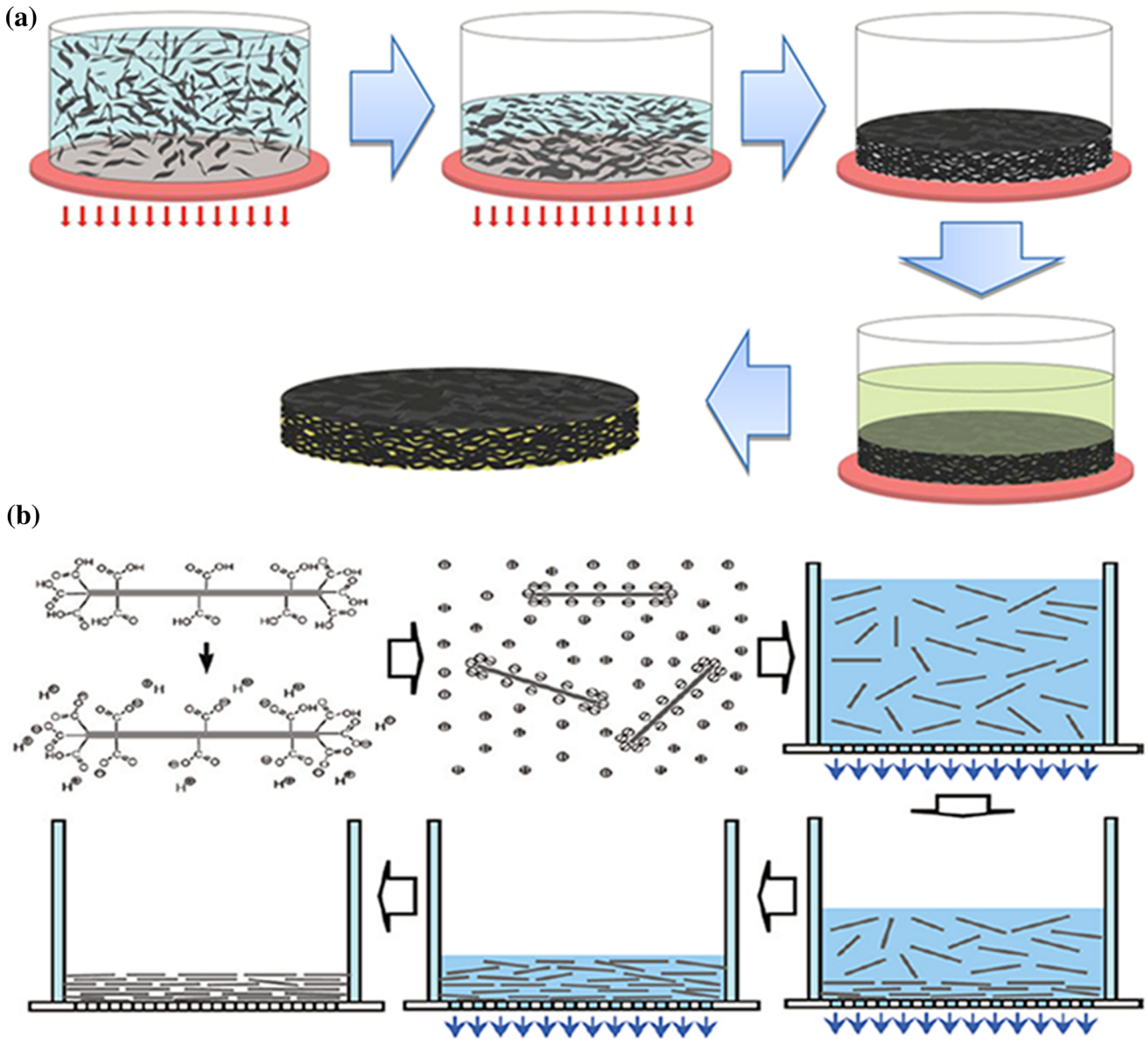

Figure 5 **a** Approach (i) and **b** approach (ii) for the preparation of AGCs by VF (see Refs. [44] and [46], respectively).

agent to obtain AG/EP composites [44]. With the same procedures, Xia et al. prepared aligned G-diamine composites with excellent performance for the removal of natural organic matter [47]. For the steps of approach (ii), the LMPG is prepared, and following the mixture is filtrated through a porous filter membrane to obtain AGCs. In comparison with approach (i), approach (ii) is widely applied due to its simple preparation steps. For example, Liu et al. prepared AG/PVA by filtrating the mixture of G dispersion and PVA solution [48]. Song et al. applied approach (ii) to obtain flexible film of AG/cellulose composite with excellent anisotropic thermal conductivity [49]. A notable difference between approaches (i) and (ii) is that AGCs with wider content range of G prepared by approach (i), while approach (ii) only can prepare AGCs with ultra-high G content.

Theoretical studies revealed the influencing factors of aligning G by VF. The higher α, the better the alignment through the "excluded volume" interaction will be. In other words, a high α value is a main factor for the alignment of G [49]. Moreover, the π–π stacking and the van der Waals forces between adjacent G lead to their stacking [50]. The functional degree of G also affects the preparation of AGCs by

filtration due to the interaction between adjacent amphiphilic groups on the basal plane [18]. Table 2 lists the recent studies on AGCs prepared by VF. It is worth noting that AGCs with high G contents can be prepared by VF, which is a complementary method of LC.

LBL

LBL is a simple and environment-friendly preparation technique and has been widely applied for the preparation of 1D, 2D, and 3D nanomaterials [53–55]. It offers a powerful tool for the preparation of tailored nanostructures with controlled thickness and functionality. Due to the inherent advantages of LBL, the as-obtained AGCs by LBL have been used for sensors, heterojunction, inkjet printing, hybrid lubricating films, and as anode material for lithium ion batteries [53, 55–58].

There are mainly two mechanisms for conducting LBL: non-covalent interactions and covalent interactions. Figure 6 shows both mechanisms. (1) A non-covalent interaction forms via intermolecular force between adsorbate and adsorbents, such as π–π stacking and formation of hydrogen bonding. Interestingly, π–π interaction between π-conjugated organic materials and the 2D sp^2 carbon network G is a non-modified method in theory, while the poor dispersity and inevitable gathering of unmodified G in solvents would impel G to modify. (2) Covalent interaction is the transfer, exchange, or coexistence of electrons. In contrast to approach (i), a covalent bond is formed between atoms by sharing electron pairs. Due to the good dispersity of graphene derivative in various solvents, LBL, GO, rGO, and FLG are widely applied in LBL to fabricate AGCs. However, depending on the applications of the AGCs, diverse types of G are chosen for LBL. Given the moderate combined electrics of thermotics and mechanic properties, rGO is preferably used in preparation of AGCs for high electric, thermal conductive, and mechanical applications, such as anode materials for lithium ion batteries, sensors, and TIM [55, 58]. For the improvement in mechanical properties of matrices alone, GO, which possesses similar mechanics to rGO and inexpensive cost, is in the leading material in use. The procedures of approach (i) and (2) are identical. Substrate is circularly dipped into GAD and matrix solvents and the cycle times correspond to the assembled layers of G. Therefore, the thickness and performances of the AGCs are controllable by adjusting the assembled times. For instance, the AG/PVA membranes were fabricated by circularly dipping hydroxyl group modified quartz substrates into PVA solution and GO solution [59]. The resulting 300-bilayer AGCs achieved improvements of 98.7% and 240.4% in elastic modulus and hardness, respectively.

Approaches (i) and (ii) can be used simultaneously in many cases. PDDA and PSS, two types of polyelectrolytes, are prevalently used in terms of LBL [60]. In light of the charge distribution (positive or negative) of the G surface, PDDA (PSS) was selected to adsorb on the surface via electrostatic interaction. In the meantime, the functional groups on G would interact with the macromolecule long chain via non-covalent interactions (dispersion force, induction force, hydrogen bond, and π–π bond). Kirschner et al. demonstrated that the strongest driving forces in LBL are covalent interactions [61].

Table 3 summarizes the various ACGs prepared by LBL in recent years. It shows that preparing 2D films by covalent interactions is the mainstream technique due to the facile control of the thickness by times of replication. The complex 1D and 3D structures of AGCs limit the development of preparing AGCs by LBL. LBL mainly offers a facile way to prepare

Table 2 AGCs prepared by VF

Type of G	Polymer solution	Size of G	VF approach	References
MG	EP monomer solution	30–80 μm	(i)	[44]
Sodium dodecyl benzene Sulfonate modified G	PVA solution	~1 μm	(ii)	[48]
GO	Cellulose solution	–	(ii)	[49]
rGO	Tween 20	–	(ii)	[51]
G	EP-20 resin	–	(i)	[52]

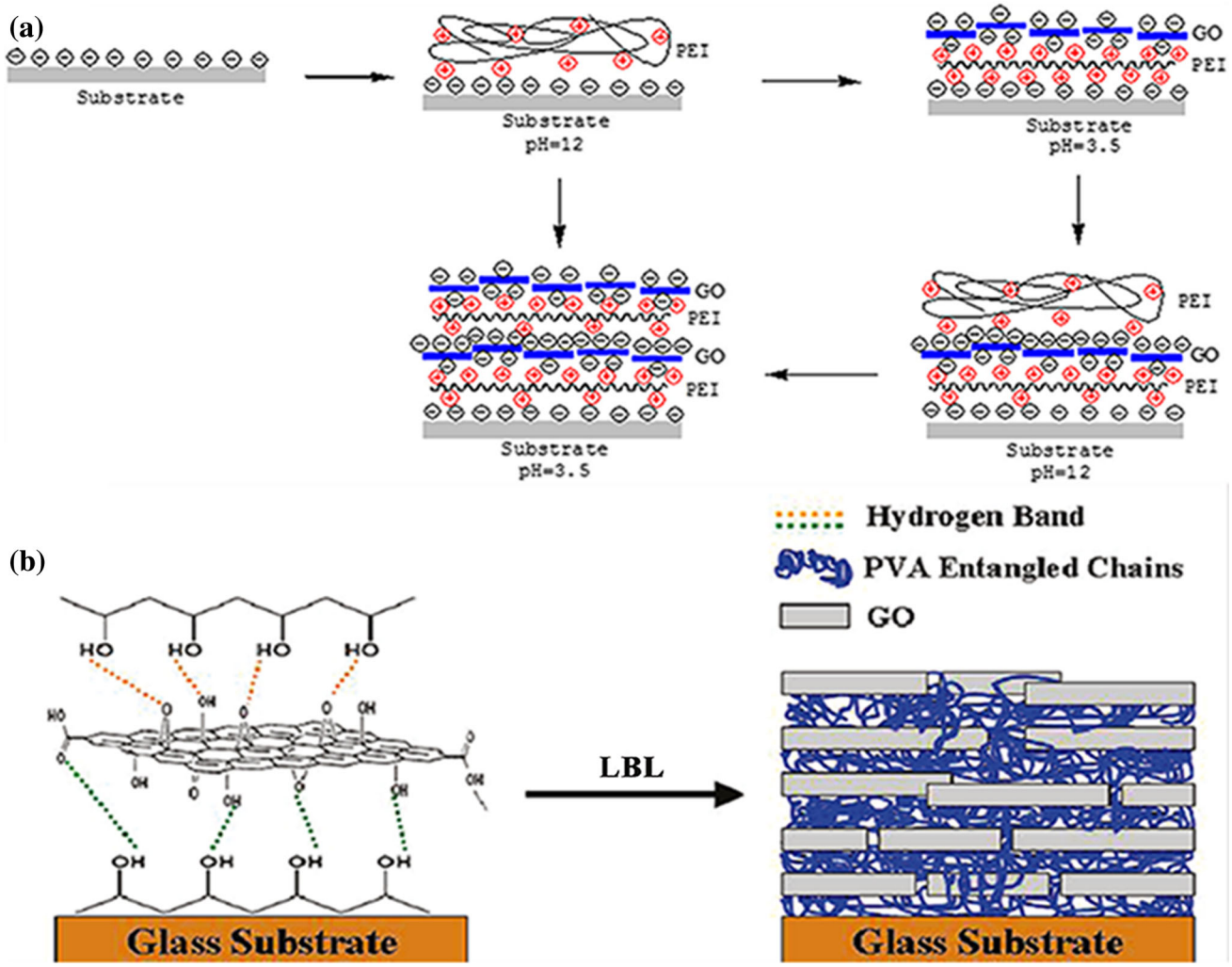

Figure 6 Mechanisms of **a** covalent interactions and **b** non-covalent interactions. (see Refs. [54] and [59], respectively).

controllable properties of AG film composites that can be applied in diverse fields.

SEI

Inspired by the preparation of G paper with layer-by-layer stacked structure [72–74], SEI, a method of aligning G by induction of solvents evaporation, has been developed for the synthesis of AGCs. From this point, under the effect of solvent evaporation, G would be subjected to a uniform upward orientation force, which leads to stacks at a near horizontal or vertical manner in the air–liquid interface. The most remarkable advantage of SEI is that the properties, such as thermal conductivity and electric conductivity, can be regulated by precisely controlling the AGCs thickness. Furthermore, the thickness of AGCs can be regulated via the added quantity of G. The facile maneuverability is a further merit of SEI. Based on both advantages, these types of AGCs were widely applied in electrode [75], sensors [76], and FETs [77]. The AGCs prepared by SEI consists of two categories: (1) AGLCs and (2) MGACs.

For the preparation of AGLCs, the procedures start with uniformly coating the substrates with DAG. Then, an AG film forms via evaporation of the solvents. The compression of the AG film follows this stage. Several parameters influence the formation and properties of the AG film. In general, the order and degree of the stacked G layer structure and the integrity of the film increase with increase in addition of G. Additionally, the usages of surfactants are a central element for the formation of AG film on substrates. Research verified that no G films can be obtained when CTAB and SDS are employed as

Table 3 Summary of various AGCs prepared by LBL

Type of G	Matrix	Approach	Application	Structure	References
GO	3,7-bis(5-(2-ethylhexyl)thiophen-2-yl)dithieno[2,3-b:2',3'-e]pyrazine	(i)	Heterojunction	Microribbon (1D)	[53]
GO	Polyethyleneimine	(ii)	–	Film (2D)	[54]
G	Polyethylene terephthalate	(ii)	Cancer sensor	Film (2D)	[55]
GO	SnO_x	(ii)	Anode material	Sandwich-like (2D)	[58]
Exfoliated G	PVA	(i)	–	Film (2D)	[59]
rGO	Poly(diallylimethyammonium chloride)	(ii)	Humidity sensor	Film (2D)	[60]
GO	Gold nanoparticles	(ii)	Enhanced Raman scattering activity	Film (2D)	[62]
GO	Zinc oxide	(ii)	Humidity Sensor	Film (2D)	[63]
Phytomolecular modified G	EP	(ii)	–	Hedgehog like bulk (3D)	[64]
rGO	Polyacrylamide	(i) and (ii)	Conductive Composite Films	Film (2D)	[65]
GO	Polyelectrolytic	(ii)	Humidity sensor	Film (2D)	[66]
Negatively charged GO	Polyolefin	(ii)	Oxygen barrier	Film (2D)	[67]
GO	Regenerated cellulose	(ii)	Enhanced mechanics	Film (2D)	[68]
GO	Poly(diallyldimethylammonium chloride)	(i) and (ii)	Humidity sensor	Film (2D)	[69]
GO	Poly(sodium 4-styrenesulfonate) / poly(allylamine hydrochloride)	(i) and (ii)	Fibroblast cell affinity	Film (2D)	[70]
rGO	TiO_2	(i)	Enhanced mechanics	G wrinkles (3D)	[71]

surfactants of G, and small-size AG films formed when SLS is used as surfactant [78]. For instance, Malekpour et al. deposited AG film on the PET substrate by using nonionic polymer-type surfactant dispersed G ink and then compressing the AG film with a compression roller. The resulting composites showed potential application as a photoelectricity technique due to the significant improvements in thermal conductivity along the IPD [77]. However, in many cases, due to the good dispersity of GO, rGO, and FLG in solvents, no surfactants are added. Using similar procedures, Kim et al. synthesized flexibly aligned rGO FETs. The FETs were operated at low voltages of < 2 V with a hole and electron mobility of 214 and 106 cm^2/V s, respectively [79]. With regard to the properties of G film, the compression procedure will improve the thermal and electric conductivity because this step can enhance the contact of G. (The detailed mechanisms are discussed in "Properties of AGCs" section.) Compared to the preparation of AGLCs by CVD, the SEI offers large-scale production capability and allows for designing G film directly onto substrates without transfer steps; however, the drawback is the relative low quality of G film due to surface modification, which decreases the intrinsic properties of G.

Similar to the VF, the preparation steps of the MGAs by SEI also include two steps. Preparing the LMPG and evaporating the solvents are both required to obtain the MGAs. Current reports showed that the G content is an important parameter for the control of the formation of AG [78]. G and GD tend to be arranged in disorder when the added amount is low. When the G content is high, the steric hindrance and excluded volume are more obvious, making G tend to stack orderly at the air-liquid interface. In addition to that, the evaporation rate of solvents is vital for the array of G. Low evaporation speed corresponds to a low induction force, which can align G parallel to substrates, whereas a high evaporation rate aligns G vertical to substrates [80]. Experiments showed that AG (parallel to substrate) formed in the G/SBR system at a curing temperature of 30 °C and concentrations of G above 1 wt%; AG

(vertical to substrate) formed at a curing temperature above 60 °C [80]. Fan et al. prepared AG/PVDF (AG parallel to substrate) composites by evaporating the LMPG solvent (*N*,*N*-dimethylacetamide) under 60 °C. The prepared composites showed a high dielectric constant (7940) when the cooperation of rGO was 0.0177 vol% [81].

UFC

The freeze-casting technique with traits of versatility, facile accessibility, and capability of producing materials with complex shapes and structures, is extensively used to fabricate 3D GA and GA composites [82, 83]. In addition to the afore-mentioned advantages of the freeze-casting technique, the resulting materials with porous structure, ultra-low density, and promising interface connection between G attract tremendous attention [84]. By regulating experimental parameters such as freeze temperature and the degree of super-cooling, a peculiar morphology and structure can be engineered [85]. In particular, the porosity, ultra-low density, and robust AG network and AGCs were designed by a modified freeze-drying process named UFC. A critical step of the UFC is the control of orientated growth of dispersing medium crystallization via high temperature gradient. The formation mechanism of the AG 3D network by UFC is shown in Fig. 7. An ultra-high degree of super-cooling can promote crystal growth along the orientation of the maximum temperature gradient, and can restrain the possible growth of secondary dendrites [86]. Furthermore, the rapid growth of dispersing medium crystallization can remove G and polymer solutions from crystals, and the removal reaction forces G to array parallel to the growth direction of the crystal. In recent years, liquid nitrogen has been employed to generate nearly 200 °C degree of super-cooling. Typically, the bottom of LMPG (DAG) is placed onto liquid nitrogen, while the roof is in contact with room-temperature air. The degree of super-cooling of the dispersing mediums is the difference between the theoretical crystallization temperature and the temperature of liquid nitrogen (~196 °C). Moreover, the concentrations of G also affect the construction of 3D AG structure [87]. Only if the concentration overtops the percolation threshold, G forms an architecture of continuous, well-interconnected, and aligned pores [88]. It has been reported that an AG network would form when the GO concentration of DAG is above 1 mg/mL [89]. The UFC also comprises two approaches to synthesize AGCs. Approach (i): frozen GAD are freeze-dried to obtain an AG aerogel into which the aimed matrices are then filled. Li et al. followed approach (i) prepared AG/EP composites with excellent EMI shielding efficiency [90]. Approach (ii): freezing the LMPG directly followed by freeze-drying to obtain AGCs. In contrast to bulk AGCs from approach (i), AGCs with porous morphology can be prepared by approach (ii). With approach (ii), Vickery et al. prepared porous and ultra-low-density AG/PVA composites with excellent mechanical properties [91], while Wang et al. prepared AG/PVA composites with analogous structures with benign dielectric properties [92].

Recently, the distinctive 3D AG structure has attracted extensive attention in the preparation of

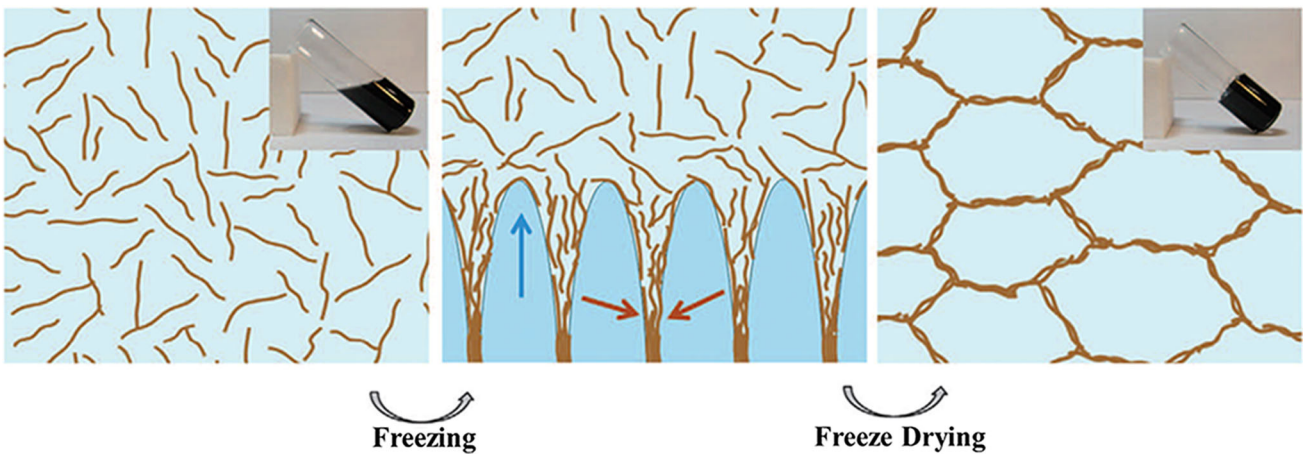

Figure 7 Mechanism of the UFC method for constructing 3D AG. (see Ref. [87]).

high-performance electrodes because the porous AG structure can provide rapid ion diffusion and high electric conductivity and can buffer the expansion of electrode materials (such as silicon and SnO_2) during the transversion of alloying [93]. To date, vertical AG (vertical to the collector) electrodes were synthesized by high-cost PECVD [94]. The AGCs prepared by approach (ii) possess high conductivity, orientation degree of G, and mechanical stability. Therefore, UFC is a promising alternative to PECVD for the preparation of vertical 3D AGCs. Despite the afore-mentioned advantages of UFC, the obvious drawback of the requirement of ultra-high super-cooling in the progress hinders its large-scale application.

Preparations of metal-based AGCs

The above-mentioned methods are for the preparation of AG/polymer composites. In recent years, researchers have developed effective methods to synthesize metal-based AGCs due to their high thermal and dimensional stability and the superior strength of metals compared to polymers. Inspired by nature, biomimetics implement the insights into researchers to array G in metals. The "brick and mortar" structure of natural nacre with nearly 95% hard mineral aragonite as "mortar" and about 5% soft protein as 'brick' was simulated to construct metal-based AGCs. Until now, both RPS and VFSPS have been developed mainly to synthesize metal-based AGCs with a "brick and mortar" structure [95, 96]. The procedures of RPS are shown in Fig. 8a. Metals are used to replicate layered porous structure materials, adsorb the G inside of porousm and press the embodied G porous metal structure to obtain AGCs. Xiong et al. employed copper to chemically replicate fir wood with a layered porous structure and the prepared AG/copper composites significantly enhanced the obtained mechanical properties [95]. For the steps of VFSPS, G was adsorbed on the surface of metal micron particles by filtrating a mixture of metal powder and GAD, and then consolidating the bulk powder mixture by SPS (see Fig. 8b). Following the VFSPS, AG/copper composites were obtained with excellent mechanical, electronic, and tribological performance [96–98]. In addition to PRS and VFSPS methods, complicated CVDS which consist of two steps was developed to prepared AG/metal composites. For example, Kim et al. and Gao et al. prepared AG/copper composites with excellent mechanics and electronic conductivity [99, 100]. However, CVDS is a rarely used method for the preparation of metal-based AGCs. Most metals (excluding Cu, Ni, and their alloys) are incapable of directly growing G, suggesting that CVDS can prepare Cu-based, Ni-based, and Cu/Ni alloy-based AGCs without transferal of G to the surface of other metals. Moreover, it is difficult to prepare metal-based AGCs with uniformly distributed nano-level AG because the large-size G film forms by CVD.

In summary, for the preparation of metal-based AGCs reported so far, copper is only used for the matrix due to the following two reasons: Copper powder possesses high chemical stability in the air environment, and it is favorable that copper powder does not form a copper oxide film on the surface of copper particles in the procedures. Furthermore, when using copper oxide powder as precursor, it reduces easily. Due to the disadvantages of the copper matrix, such as high density and poor corrosion resistance in the alkaline environment, more metal matrices should be developed to meet the requirements of applications and industries. Furthermore, the discussion of influencing factors and the establishment of a theoretical model should also be achieved to enable the precise control of preparation procedures.

Properties of AGCs

Electrical conductivity

Based on the electric conductive percolation theory, the conductive network formation of fillers is an important condition for enhancing the electric conductivity of composites. In general, the value of increasing volume fraction of conductive fillers to a critical value and an insulator-to-conductor transition occurs (Pc) and σ are two parameters used for the evaluation of the electric performances of polymer composites. A desirable lower Pc and higher σ at lower addition of G mean that lower consumption of the expensive G can achieve higher electric conductivity performances. For metal-based composites, the percent increase of σ is used as evaluation criterion.

As a conductive nanofiller with ultra-high σ and α, G has been considered as an ideal conductive filler. In particular, the arrangement of G in matrices affects the construction of the conductive network and the

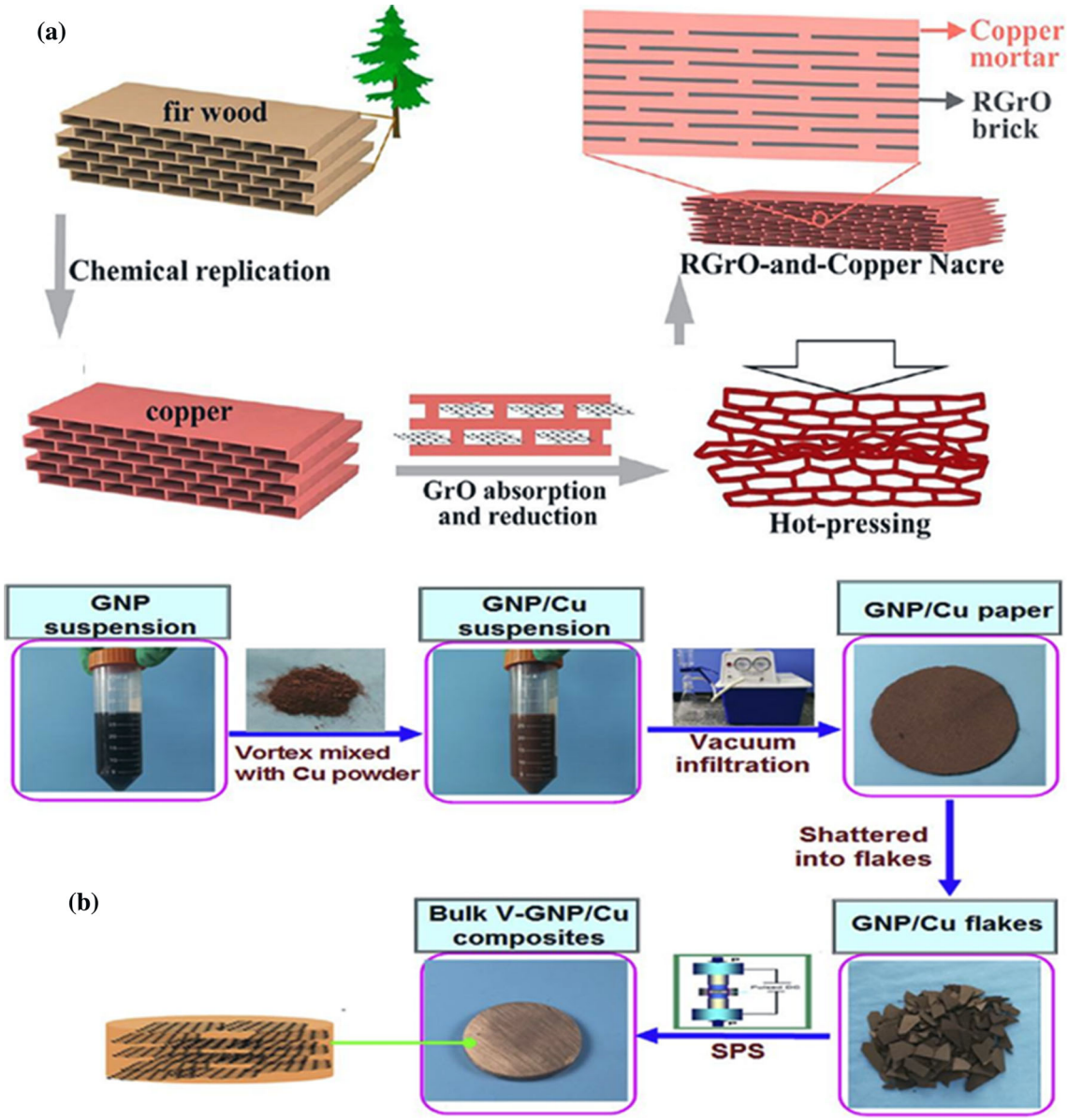

Figure 8 Mechanism of **a** PRS (Ref. [95]) and **b** FSPS (Ref. [96]) progresses.

conductivity of composites. Because the electric conductivity of G at IPD is higher than that at TTD, the array can fully utilize their electric conductivity [23]. Furthermore, a large body of work indicated that the AG would facilitate the formation of a conductive network. Various matrices, such as PU [22], EP [18], PVDF-HFP [25], cellulose [68], SBR [80], PVDF [81], and copper [99] have boosted electric conductive properties via the alignment of G, and the resulting AGCs demonstrated lower Pc and higher σ in the orientation of the aligned G. For example, the Pc (0.22 vol%) of AG/EP composites was twofold higher than that of RG/EP composites, and the σ of AG/EP composites increased by nearly two orders of magnitude compared to that of RG/EP composites [41]. In addition, experiments showed that the electric properties of RG/EP composites and AG/EP composites at TTD are almost identical [41]. An effective-medium theory of σ for AG/polymer composites has been developed [14], demonstrating that aligning G is a better way to improve the resulting electric properties, as well as achieving the conductive applications of AP/EP composites. The comprehensive electric property of AGCs outperforms that of RGCs.

Several intrinsic properties of G significantly affect the electric properties of AGCs: (1) the presence of

functional groups on G. The more functional groups there are, the lower σ will be. Basically, the introduction of groups onto G can damage the inherent sp^2 structure, which then rapidly decreases the σ of G. For example, Yousefi et al. showed that aligned GO composites functioned as an insulator even if the addition of GO was as high as 3 wt% [18]. (2) The dispersity of G in matrices. Good dispersity implies that the formation of a conductive network is possible even at low G addition. However, it is well known that G inevitably gathers in matrices without modification. By adsorbing surfactants and anchoring functional groups onto G, G obtains good dispersity, while it decreases their σ. To address this contradiction, rGO, with the have combined performances of moderate dispersity and σ, is widely used in conductive AGCs as a compromising strategy [25, 78, 80]. (3) Size of G. The σ of large-area G is higher than that of small-area G because large-area G possess smaller inter-sheet contact resistance in matrices [101]. Kumar et al. exhibited large-area reduced-AG/PVDF-HFP composites, the σ of the composites was obviously higher than that of small-area reduced-AG/PVDF-HFP composites [25].

Here, we summarize and compare the electric properties of RGCs and AGCs for different directions. As shown in Table 4, the results mostly correspond to the presented viewpoints, although the Pc and σ are strongly influenced by a number of factors. Aligning G into matrices is a more effective way to enhance the electric performance of composites.

Mechanical properties

G is considered to be one class of the emerging enhanced phases for various matrices due to their incomparable mechanics and ultra-high α, that can effectively boost the mechanical performance of matrices when the additional content is low. Figure 9 shows the AG enhancement mechanisms for both polymer-based and metal-based composites. It is reasonable to assume that the introduction of AG is a more effective way to improve the mechanical performances for matrices than RG because flake-like G can bear loads only at the IPD. Furthermore, the arranged G can effectively inhibit the slip of the polymer chains in AG/polymer composites [107] and the plane slip in AG/metal composites [99].

Therefore, theoretically, the orientation distribution of G in matrices has a pivotal effect on the improvement of mechanics [110]. A large number of studies investigated the array of G in various matrices, such as PI [22], chitosan [19], PU [20, 22], EP [18], Tween [51], and copper [99], to enhance mechanics. To date, because most of the presented studies focused on the increase in tensile strength and elastic modulus, we, therefore, discuss the reinforcement mechanisms of AGCs for tensile strength and elastic modulus.

Based on the Halpin–Tsai model [108], the moduli of AGCs are theoretically calculated by Eqs. (2–3):

$$E = E_{\mathrm{m}}\left(\frac{1+\gamma_1\beta V_{\mathrm{f}}}{1-\gamma_1 V_{\mathrm{f}}}\right) \tag{2}$$

$$\gamma_1 = \frac{\frac{E_{\mathrm{f}}}{E_{\mathrm{m}}}-1}{\frac{E_{\mathrm{f}}}{E_{\mathrm{m}}}+\beta}, \quad \beta = \frac{2\alpha}{3} \tag{3}$$

Here, E, E_{m}, and E_{f} represent elastic moduli of AGCs, matrices, and fillers respectively, and V_{f} represent the volume fraction of G in Eqs. (2–3). Since E_{f} and α are directly proportional to E, the ultra-high elastic modulus and α of G have intrinsic superiority as oriented enhanced phases. In addition to the aforementioned influencing factors, the interfacial interaction between G and matrices also plays a key role in the improvement of mechanics. The stronger interfacial interaction leads to better reliable transfer of the loads between matrices and G. The formations of covalent bonds, hydrogen bonds, and π–π bonds have been applied between matrices and G to enhance the interfacial interaction. Establishing chemical bonds between functional groups of G and polymer monomers during the procedures of polymerization of polymer normally reduces GO. Yousefi et al. expounded the detailed reaction mechanism of GO and EP monomers in procedures of in situ polymerization, and using a modulus as high as 800 MPa resulted in AG/EP with 2 wt% GO, which demonstrated a strong interfacial interaction between GO and EP [18]. The contained oxygen, nitrogen, and fluorine functional groups on G and polymer matrices probably form strong hydrogen bonds. The prime formation mechanism of hydrogen bonds mainly includes highly polar polyalcohols and G in a G/polymer system. Huang et al. explained the formation of hydrogen bonds between hydroxyl of PVA and oxygenated groups of GO by a shift of vibration peak position [109]. G and many polymers with abundant aromatic rings are an important prerequisite for the improvement of the interfacial bonding by

Table 4 Electric properties of RGCs and AGCs

Type of G	Matrix	Pc		σ (S/cm)		Type of composite	Size of G	Preparation method	References
		IPD	TTD	IPD	TTD				
rGO	PU	0.078 vol%	–	$\sim 10^{-3}$ (5 wt%)	–	AGCs	32.7 ± 24.3 μm	LC	[23]
rGO	EP	0.23 vol%	–	$\sim 10^{-2}$ (3 wt%)	$\sim 10^{-5}$ (0.75 wt%)	AGCs	$\sim 120\ \mu m^2$	LC	[24]
GO	EP	–	–	$\sim 10^{-11}$ (3 wt%)	$\sim 10^{-11}$ (3 wt%)	AGCs	$\sim 180\ \mu m^2$	LC	[24]
rGO	PVDF-HFP	1.37 wt%	–	$\sim 3 \times 10^3$ (25 wt%)	–	AGCs	$\sim 25\ \mu m^2$	LC	[25]
rGO	PVDF-HFP	1.32 wt%	–	$\sim 2 \times 10^3$ (25 wt%)	–	AGCs	$\sim 5\ \mu m^2$	LC	[25]
rGO-Fe_3O_4	PAMPs	10 vol%	–	$\sim 2 \times 10^{-2}$ (2 vol%)	–	AGCs	–	EMF	[36]
G	EP	0.22 vol%	0.52 vol%	$\sim 10^{-7}$ (1.6 wt%)	$\sim 10^{-7}$ (1.6 wt%)	AGCs	~25 μm	EEF	[41]
G	SBR	0.13 wt%	–	3.70 (15 wt%)	2.56×10^{-5}(15wt%)	AGCs	~1.3 μm	SEI	[80]
rGO	PVDF	0.0018 vol%	–	$\sim 10^{-5}$ (0.035 vol%)	–	AGCs	–	LC	[81]
G	EP	0.007 vol%	0.007 vol%	0.17 (~ 0.17 vol%)	~0.01 (~ 0.17 vol%)	AGCs	~202 μm	UFC	[89]
G	Copper	–	–	~58	–	AGCs	–	CVDS	[99]
rGO	UHMWPE	2–3 wt%		~10 (40 wt%)		RGCs	~5 μm	Dry-mixed	[102]
Thermally rGO	PU	~0.5 vol%		–		RGCs	–	Melt compounding	[103]
KH550-G	PEEK[c]	~0.2 vol%		$\sim 10^{-4}$ (5.5 vol%)		RGCs	~2 μm	Solution mixing	[104]
Thermally rGO	PEEK	~0.76 vol%		$\sim 3 \times 10^{-3}$ (4 vol%)		RGCs	~2 μm	Solution mixing	[105]
rGO	PU	~0.3 wt%		$\sim 10^{-5}$ (4 wt%)		RGCs	~2 μm	Solution mixing	[105]
rGO	Rubber	~0.62 vol%		$\sim 10^{-2}$ (9 vol%)		RGCs	~1 μm	Latex mixing	[106]

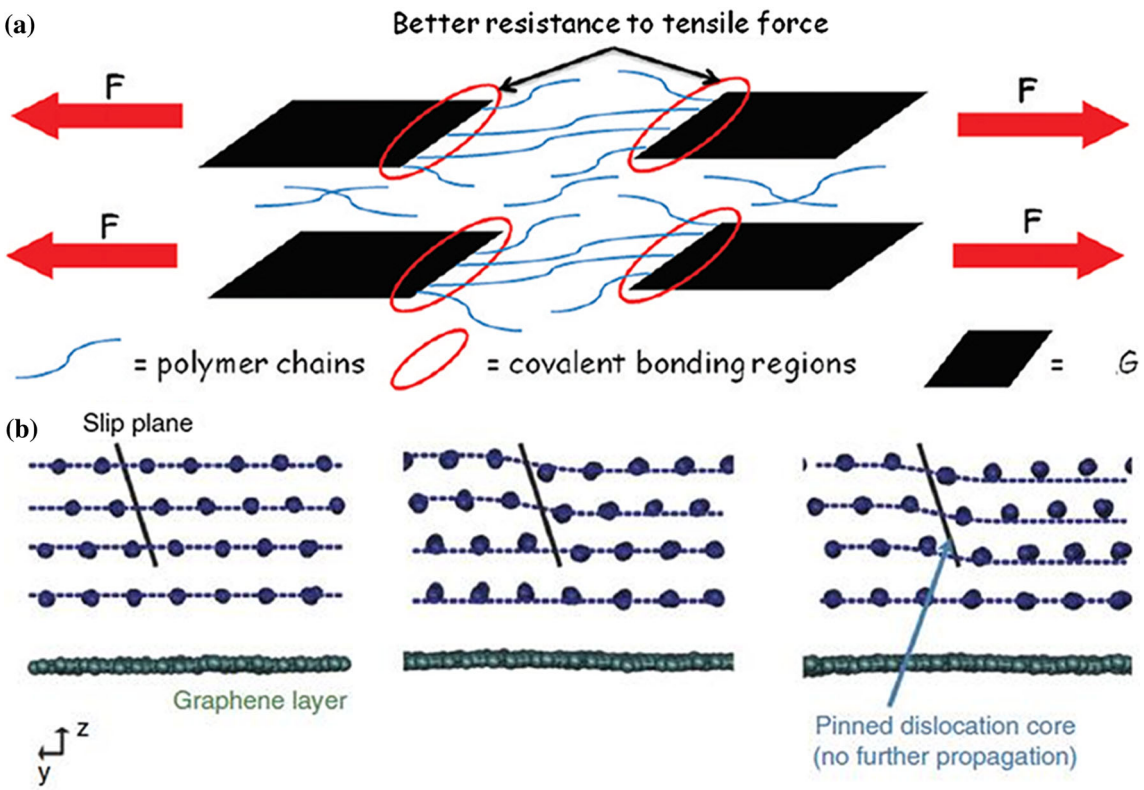

Figure 9 **a** AG enhancement mechanism for polymer-based composites and **b** AG inhibits the plane slip mechanism in metal-based composites. (Refs. [107] and [100], respectively).

π–π stacking, as has been reported by PEDOT and GO [110]. As an unavoidable problem, the dispersity of G in matrices also significant affects the improvement of the resulting mechanics. With increasing G content, the moduli and strength of AGCs showed a first increasing and then decreasing trend in most relevant studies, as a result of the unavoidable gathering at high contents, while leads to a decrease of load transfer.

Table 5 summarizes and compares the elastic modulus and tensile strength of AGCs and RGCs with different G contents by various preparation methods. Although the mechanic improvement in composites is strongly influenced by the matrices, G types, and preparation methods, AGCs possess higher mechanics than RGCs.

Thermal properties

In addition to the high phonon λ of honeycomb-like G as a result of the strong covalent bonds, the super-high α and thermal stability, which can minimize the thermal interface resistance, indicate G as an ideal thermal conductive enhanced filler. Similar to the improvement in σ, the G network plays the role of thermal conductive channels in composites. AG can facilitate the formation of the thermal conductive network and noticeably decrease the thermal interfacial resistance between G and matrices. The thermal conductive mechanism is shown in Fig. 10. Renteria et al. reported that the thermal properties of AG/EP composites far exceeded those of RG/EP composites [37]. Moreover, aligning G with anisotropic λ, ultra-high 2000–5000 W/mK along the IPD or 10–20 W/mK along TTD [119], can make the best use of G as a 2D material as well as can provide the possibility for designing AGCs with extraordinary λ at the aligned G orientation. The anisotropic thermal conductive AGCs are hopefully applied in TIM, dissipating materials [37, 52, 120–123], which have a strong requirement for oriented heat conduction. The thermal properties of AGCs and RGCs are listed in Table 6. The summarized reasons indicate that AGCs have better thermal properties.

Table 5 Elastic moduli and strength of AGCs and RGCs

Type of G	Matrix	Maximal increase in strength (%)	Maximal increase in elastic modulus (%)	α or size of G	Preparation method	Type of composites	References
GCA	PI	–	27% (0.8 wt%)	–	LC	AGCs	[24]
GO	Chitosan	93% (1 wt%)	51% (1 wt%)	~876 m^2/g	LC	AGCs	[19]
rGO	PU	2100% (3 wt%)	900% (3 wt%)	13500	LC	AGCs	[20]
GO	EP	500% (1.5 wt%)	70% (1.5 wt%)	–	LC	AGCs	[18]
rGO	EP	~350% (1.5 wt%)	~50% (1.5 wt%)	–	LC	AGCs	[24]
GO	PEM/PSS/PAH	–	~500%	–	LBL	AGCs	[70]
rGO	Copper	~41% (1.2 vol%)	~12% (1.2 vol%)	0.2–2 μm	PRS	AGCs	[95]
G	Copper	~73.4% (2.5 vol%)	~25% (2.5 vol%)	–	CVDS	AGCs	[99]
G	Copper	32–51%	–	–	CVDS	AGCs	[100]
G	Copper	~130% (0.6 vol%)	65% (0.8 vol%)	5–15 μm	FSPS	AGCs	[111]
PSS-G	PVA	~350% (2 wt%)	–	~300 nm	UFC	AGCs	[91]
GO	SBR	~800 (3 wt%)	~545% (3 wt%)	–	LC	AGCs	[112]
BTESPT-GO	Natural rubber	~100 (0.3 wt%)	–	~1 nm	Solution mixing	RGCs	[113]
rGO	Natural rubber	48% (0.5 wt%)	80% (0.5 wt%)	–	Latex mixing	RGCs	[114]
rGO	CA	102% (1.5 wt%)	143 (1.5 wt%)	–	Solution mixing	RGCs	[115]
PS-GO	SSBR-BR	~23% (0.5 wt%)	Basically the same	–	Two-roll mill	RGCs	[116]
PSI-GO	SSBR-BR	25% (0.5 wt%)	Basically the same	–	Two-roll mill	RGCs	[116]
GO	Copper	11% (0.3 wt%)	–	–	Sinter	RGCs	[117]

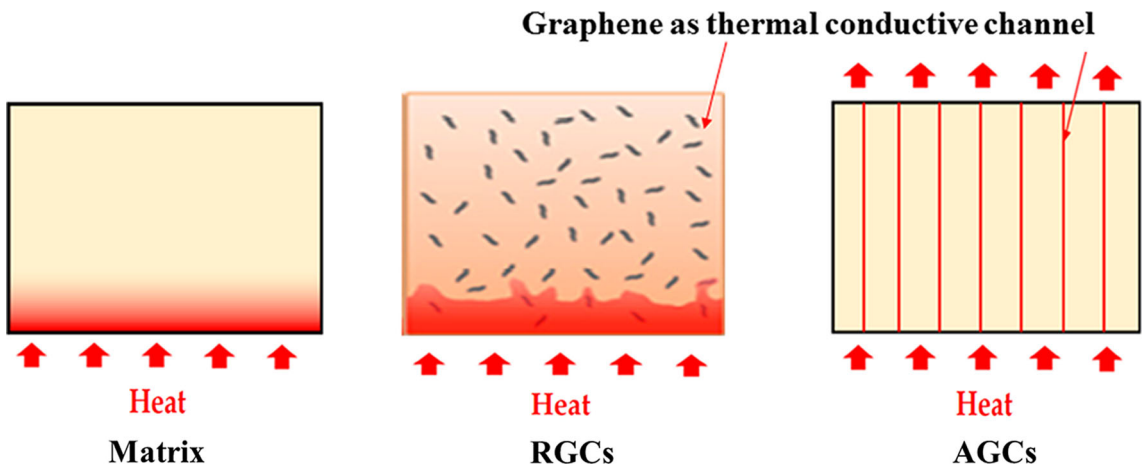

Figure 10 Thermal conductive mechanism of pure matrix, RGCs, and AGCs. (Ref. [118]).

Anti-corrosion properties

In the natural environment, H_2O, O_2, and Cl^- are the nemesis of corrosion in most materials. Therefore, isolating the metal interface from the electrolyte is a rational way to protect materials from corrosion by introducing organic coating at the surface of materials [132]. However, the anti-permeability properties of pure organic coatings are poor. The combination with fillers for polymer coatings is an effective method to enhance their anti-corrosion properties. G with high α, chemical inertness, and excellent anti-permeability (only protons can pass through) have inspired considerable work to utilize G/polymer composites as anti-corrosion coatings [133–135]. A proven theory indicates that the cooperation of G strongly increases the diffusion pathway of the electrolyte from the surface of coatings to the metal

Table 6 Thermal properties of AGCs and RGCs

Type of G	Matrix	% increase in λ/(W/(mK))		Type of composite	Preparation method	References
		IPD	TTD			
rGO	PVDF-HFP	~8700% (27.2 wt%)	–	AGCs	LC	[25]
G-Fe_3O_4	EP	~139% (1 vol%)	~50% (1 vol%)	AGCs	EMF	[34]
G-Fe_3O_4	EP	~117% (0.52 vol%)	–	AGCs	EMF	[37]
Multilayer G	EP	~15100% (11.8 wt%)	~173%	AGCs	LBL	[44]
G	PVA	36.81 W/(mK) (65 wt%)	–	AGCs	VF	[44]
rGO	Cellulose	6.2 W/(mK) (–)	0.072 W/(mK) (–)	AGCs	VF	[46]
G	EP	~490% (44 vol%)	~218% (44 vol%)	AGCs	VF	[52]
G	EP	~0.45 W/(mK) (0.108 vol%)	~0.41 W/(mK) (0.108 vol%)	AGCs	EEF	[41]
G	PET	~90 W/(mK) (–)	–	AGCs	SEI	[77]
G	Copper	~50% (35 vol%)	~− 75% (35 vol%)	AGCs	VFSPS	[96]
G	Copper	~35% (30 vol%)	–	AGCs	VFSPS	[98]
Multilayer G	EP	~5.2 W/(mK) (–)		RGCs	Solution blending	[120]
GO	Copper	~13% (–)		RGCs	Sintering	[117]
VTMS-GO	Silicone polymer	~78.3% (0.5 wt%)		RGCs	Solution mixing	[124]
G	EP	~36% (2 wt%)		RGCs	Latex mixing	[125]
GO	EP	~105% (1 wt%)		RGCs	Latex mixing	[126]
rGO	EP	~72% (1 wt%)		RGCs	Latex mixing	[126]
G	PVDF	100% (2 wt%)		RGCs	Solution blending	[127]
G	Perfluoroalkoxy	2188% (20% wt%)		RGCs	Hot-pressed	[128]
G	Polyvinyl butyral	~1491 (25 wt%)		RGCs	Solution blending	[129]
FLG	PI	~400% (5 wt%)		RGCs	Electrospinning–hot press	[130]
G	Copper	~12% (1 vol%)		RGCs	Sintering	[131]

interface [136, 137]. Moreover, experiments have shown that the alignment of G would strongly affect the anti-corrosion properties of coatings because AG (vertical to the direction of electrolyte diffusion) can effectively increase the diffusion pathway. The anti-corrosion mechanisms of AGCs and RGCs are shown in Fig. 11. Luo et al. reported that the AG/EP anti-corrosion property far exceeded that of RG/EP coating [138]. Li et al. synthesized an AG/PU anti-corrosion coating via the LC method, and verified that the anti-corrosion performance of AGCs was higher than that of RGCs vis EIS analysis [21]. Because the anti-permeabilities of G and GO are nearly identical, GO with high processability and dispersibility in aqueous media was widely applied in anti-corrosion coatings [132, 139, 140]. However, reported studies on anti-corrosion of AGCs are limited, due to the undeniable difficulty for the preparation of AGCs on the surface of materials by the afore-mentioned methods.

Trinological property

Graphite carbon including G has been found to have outstanding tribological properties [141]. Furthermore, many studies indicated that AG can fully utilize the self-lubricating property of 2D material [32, 142]. Several mechanisms have been developed to explain the excellent tribological properties of AGCs: (1) AGCs can boost the contact area between AG and friction counterparts. (2) AG facilitate the formation of G transform film on friction

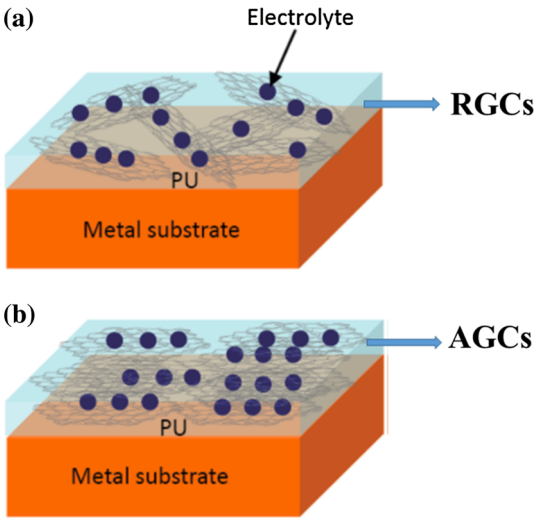

Figure 11 Anti-corrosion mechanisms of **a** RGCs and **b** AGCs. (Ref. [21]).

counterparts under a moderate content of G addition. The schematic is shown in Fig. 12. Both phenomena transfer the wear from between the friction counterparts and matrices to between counterparts and AG. For instance, Liu et al. prepared AG/bismaleimides composites via EMF, and the obtained composites have a friction coefficient of as low as 0.07 for an addition of G-Fe_3O_4 of 0.06 wt% [32].

Friction coefficient and volume wear rate are used to evaluate the friction properties. We summarized and compared the friction coefficient and volume wear rate of AGCs and RGCs. As shown in Table 7, the tribological performances of AGCs far exceed those of the RGCs although there are limited reports on the tribological properties of AGCs. Interestingly, additions of rGO and FGS into SSBR-BR have a side effect on the tribological properties of composites [143]. It is plausible that the existence of a disordered alignment of rGO (FSG) in rubber matrices can greatly induce tear, curling, and peeling off on worn surfaces of the composites, emphasizing the importance of AG to enhance the wear performance.

EMI shielding property

Traditional metallic coatings and cases of EMI shields with heavy weight are undesirable for their applications. G (including partial graphene derivatives) with low density, ultra-high electronic and thermal conductivity, and mechanics are indicated as ideal fillers for EMI shielding composites. The EMI shielding behavior of G primary stems from the strong electrical loss of microwaves [146, 147]. Normally, the EMI shielding performance is proportional to the σ value of G composites. In "Electrical conductivity" section, the advantages of AGCs have been discussed in electrics. However, the design of G composites with high dielectric permittivity is a further way to boost the EMI shielding property [148]. In microstructures of polymer-based AGCs, any pair of adjacent conductive G separated by an insulating polymer thin film can serve as a nanoscale capacitor. The enormous AG network, containing millions of capacitors, can hold an extremely large capacity for the storage of electric charges, thus equipping the AGCs with superior dielectric permittivity [149]. A schematic of nanoscale capacitors is shown in Fig. 13a. AGCs combine both merits of excellent electronic conductivity and the formation of numerous nanoscale capacitors, leading to the following

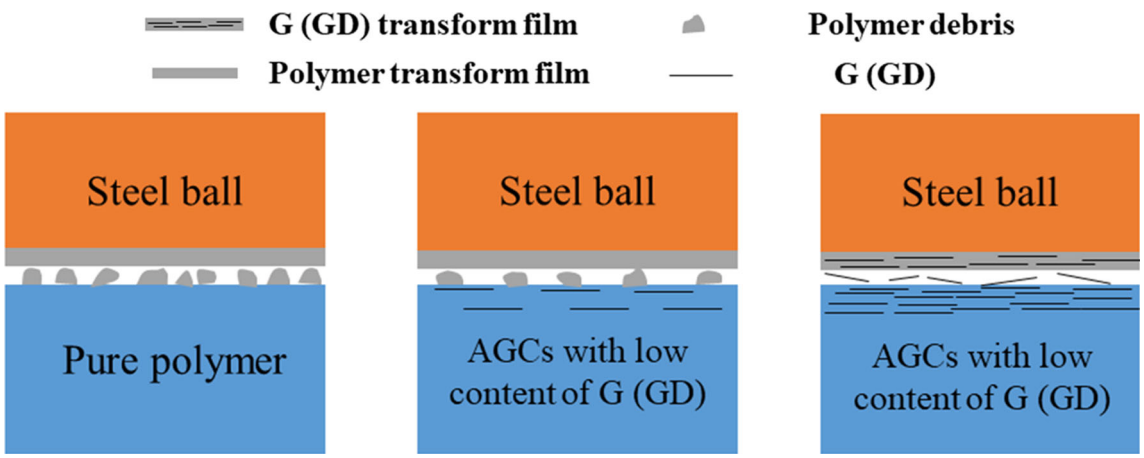

Figure 12 Tribological schematic of AGCs. (Ref. [142]).

Table 7 Tribological property of AGCs and RGCs

Type of G	Matrix	% decrease in friction coefficient	% decrease volume wear rate	Type of composite	Preparation method	References
G-Fe_3O_4	Bismaleimide	~82% (0.6 wt%)	~50% (0.6 wt%)	AGCs	EMF	[32]
G	SBR	~62% (5 wt%)	~89% (5 wt%)	AGCs	SEI	[142]
GO	Nitrile rubber	~13% (0.5 wt%)	~48% (0.5 wt%)	RGCs	Solution mixing	[141]
FGS	SSBR-BR	–	~-8% (0.5 wt%)	RGCs	Two-roll mill	[143]
rGO	SSBR-BR	–	~-3% (0.5 wt%)	RGCs	Two-roll mill	[143]
FLG	EP	~9% (1 wt%)	~45% (1 wt%)	RGCs	Solution mixing	[144]
GO	UHMWPE	Basically the same	~11% (1 wt%)	RGCs	Hot-pressing	[145]

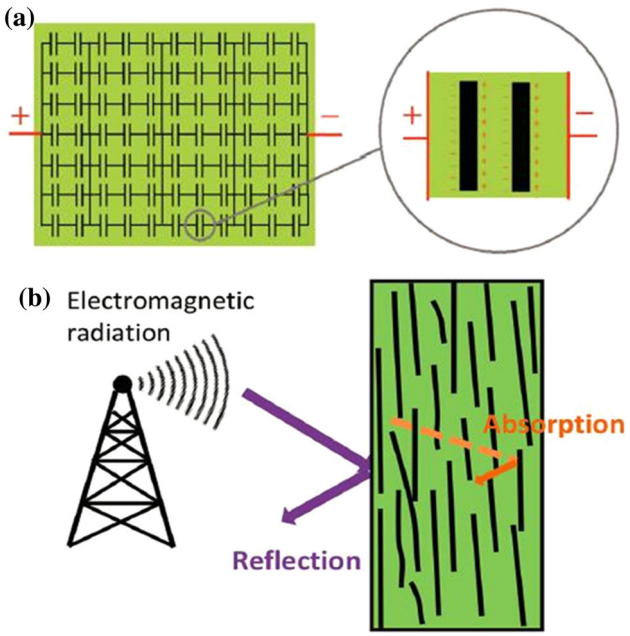

Figure 13 **a** Schematic of the formation of numerous nanoscale capacitors in G composites by AG. **b** Enhanced electromagnetic waves reflect and absorb AGCs.

two enhancements for EMI shielding performance: (1) capability of absorbing the incidental electromagnetism waves via polarization in numerous nanoscale capacitors; (2) the G aligned in IPD contributes positively to shielding the electromagnetic waves that emanate through the thickness direction by increasing the reflective area (Fig. 13b) [150]. Yousefi et al. prepared an AG/EP composite with 3 wt% of rGO via LC, and the composites exhibited a dielectric constant exceeding 14000 at 1 kHz and an EMI shielding efficiency of about 40 dB in 500–4000 MHz [149], which was far higher than similar RGCs [9, 151, 152]. Song et al. prepared an AG/wax composite via the hot-press method and the obtained AGCs presented above 30% increment in shielding effectiveness based on unaligned G/wax composite [150]. The afore-mentioned studies indicate that the cooperation of AG in polymers is a more effective means to boost the EMI shielding property of G composites.

Conclusions and prospects

In summary, the methods for preparation and the resulting properties of AGCs have been summarized. With regard to the preparation methods, each has its own merits, such as the simple procedures of LC, VF, and SEI, which limit the G content of EMF, EEF, and VFSPS little, as well as the porous structure of UFC, energy conservation of LC, VF, LBL, and SEI. Researchers can choose the most suitable method for their experiments. With regard to the properties of AGCs, the enhanced mechanisms of AGCs and influencing factors have been discussed in detail. Aligning G in matrices is an ideal method to fully utilize its excellent properties. Based on these outstanding multifunctional properties, AGCs are promising as structural and functional materials (sensors, heterojunction, inkjet printing, hybrid lubricating films, and anode material for lithium ion batteries).

However, several existing issues still need to be addressed. (1) The studies on the influencing factors of the G orientation and alignment are not thorough, especially lacking systematic mathematical models for methods such as VF, SEI, UFC, and VFSPS. (2) The macroscopical order degree of AGCs is imperfect. (3) It remains difficult to prepare more metal-based and ceramic-based AGCs. (4) The current methods for preparing AGCs need to be studied in depth, existing methods need to be constantly improved, and new

technologies for the large-scale industrial production need to be developed.

Acknowledgement

This work was supported by Supported by Sichuan Science and Technology Program (2018GZ0459).

References

[1] Novoselov KS, Fal′Ko VI, Colombo L, Gellert PR, Schwab MG, Kim K (2012) A roadmap for graphene. Nature 490:192–200

[2] Kaur K, Jeet K (2017) Electrical conductivity of water-based nanofluids prepared with graphene-carbon nanotube hybrid. Fuller Nanotub Carbon Nanostruct 25:726–734

[3] Lee Y, Bae S, Jang H et al (2010) Wafer-scale synthesis and transfer of graphene films. Nano Lett 10:490–493

[4] Nika DL, Balandin AA (2012) Two-dimensional phonon transport in graphene. J Phys Condens Matter 24:233203

[5] Nika DL, Balandin AA (2017) Phonons and thermal transport in graphene and graphene-based materials. Rep Prog Phys 80:036502

[6] Kuilla T, Bhadra S, Yao D, Kim NH, Bose S, Lee JH (2010) Recent advances in graphene based polymer composites. Prog Polym Sci 35:1350–1375

[7] Zhan Y, Wu J, Xia H, Yan N, Fei G, Yuan G (2011) Dispersion and exfoliation of graphene in rubber by an ultrasonically-assisted latex mixing and in situ reduction process. Macromol Mater Eng 296:590–602

[8] Mao Y, Wen S, Chen Y et al (2013) High performance graphene oxide based rubber composites. Sci Rep 3:2508

[9] Liang J, Wang Y, Huang Y et al (2009) Electromagnetic interference shielding of graphene/epoxy composites. Carbon 47:922–925

[10] Jafari Y, Ghoreishi SM, Shabani-Nooshabadi M (2016) Polyaniline/graphene nanocomposite coatings on copper: electropolymerization, characterization, and evaluation of corrosion protection performance. Synth Met 217:220–230

[11] Fan D, Zhang R, Wang X, Huang S, Peng H (2012) Influence of silver dopant on the morphology and ultraviolet emission in aligned zno nanostructures. Phy Status Solidi A 209:335–339

[12] Huard M, Roussel F, Rouzière S, Patel S, Pinault M, Mayne LM, Launois P (2014) Vertically aligned carbon nanotube-based composite: elaboration and monitoring of the nanotubes alignment. J Appl Polym Sci 131:1–15

[13] Nain AS, Wang J (2013) Polymeric nanofibers: isodiametric design space and methodology for depositing aligned nanofiber arrays in single and multiple layers. Polym J 45:695–700

[14] Xia X, Hao J, Wang Y, Zhong Z, Weng GJ (2017) Theory of electrical conductivity and dielectric permittivity of highly aligned graphene-based nanocomposites. J Phys Condens Matter 29:205702

[15] Shivanandareddy AB, Krishnamurthy S, Lakshminarayanan V, Kumar S (2013) Mutually ordered self-assembly of discotic liquid crystal-graphene nanocomposites. Chem Commun 50:710–712

[16] Eppenga R, Frenkel D (1984) Monte carlo study of the isotropic and nematic phases of infinitely thin hard platelets. Mol Phys 52:1303–1334

[17] Aboutalebi SH, Gudarzi MM, Zheng QB, Kim JK (2011) Spontaneous formation of liquid crystals in ultralarge graphene oxide dispersions. Adv Funct Mater 21:2978–2988

[18] Yousefi N, Lin X, Zheng Q et al (2013) Simultaneous in situ reduction, self-alignment and covalent bonding in graphene oxide/epoxy composites. Carbon 59:406–417

[19] Pan Y, Wu T, Bao H, Li L (2011) Green fabrication of chitosan films reinforced with parallel aligned graphene oxide. Carbohyd Polym 83:1908–1915

[20] Yousefi N, Gudarzi MM, Zheng Q et al (2013) Highly aligned, ultralarge-size reduced graphene oxide/polyurethane nanocomposites: mechanical properties and moisture permeability. Compos Part A Appl S 49:42–50

[21] Li Y, Yang Z, Qiu H, Dai Y, Zheng Q, Li J, Yang JH (2014) Self-aligned graphene as anticorrosive barrier in waterborne polyurethane composite coatings. J Mat Chem A 2:14139–14145

[22] Gudarzi MM, Aboutalebi SH, Yousefi N, et al (2011) Self-aligned graphene sheets-polyurethane nanocomposites. In: Mrs online proceedings library archive, p 1344

[23] Yousefi N, Gudarzi MM, Zheng Q, Aboutalebi SH, Sharif F, Kim JK (2012) Self-alignment and high electrical conductivity of ultralarge graphene oxide–polyurethane nanocomposites. J Mater Chem 22:12709–12717

[24] Kim GY, Choi MC, Lee D, Ha CS (2012) 2D-aligned graphene sheets in transparent polyimide/graphene nanocomposite films based on noncovalent interactions between poly(amic acid) and graphene carboxylic acid. Macromol Mater Eng 297:303–311

[25] Kumar P, Yu S, Shahzad F, Hong SM, Kim YH, Chong MK (2016) Ultrahigh electrically and thermally conductive self-aligned graphene/polymer composites using large-area reduced graphene oxides. Carbon 101:120–128

[26] Behabtu N, Lomeda JR, Green MJ et al (2010) Spontaneous high-concentration dispersions and liquid crystals of graphene. Nat Nanotechnol 5:406–411

[27] Ominato Y, Koshino M (2013) Orbital magnetism of graphene flakes. Phys Rev B 87:269–275
[28] Tian B, Lin W, Zhuang P, Li J, Shih TM, Cai W (2018) Magnetically-induced alignment of graphene via landau diamagnetism. Carbon 131:66–71
[29] Li D, Liu Y, Ma H, Wang Y, Wang L, Xie Z (2015) Preparation and properties of aligned graphene composites. RSC Adv 5:31670–31676
[30] Babaei H, Keblinski P, Khodadadi JM (2013) Thermal conductivity enhancement of paraffins by increasing the alignment of molecules through adding CNT/graphene. Int J Heat Mass Transf 58:209–216
[31] Babonneau D, Camelio S, Simonot L, Pailloux F, Guérin P, Lamongie B, Lyon O (2011) Tunable plasmonic dichroism of au nanoparticles self-aligned on rippled Al_2O_3 thin films. EPL 93:26005
[32] Liu C, Yan H, Chen Z, Yuan L, Liu T (2015) Enhanced tribological properties of bismaleimides filled with aligned graphene nanosheets coated with Fe_3O_4 nanorods. J Mater Chem A 3:10559–10565
[33] Yan H, Tang Y, Long W, Li Y (2014) Enhanced thermal conductivity in polymer composites with aligned graphene nanosheets. J Mater Sci 49:5256–5264. https://doi.org/10.1007/s10853-014-8198-z
[34] Renteria J, Legedza S, Salgado R et al (2015) Magnetically-functionalized self-aligning graphene fillers for high-efficiency thermal management applications. Mater Des 88:214–221
[35] Liang J, Xu Y, Sui D et al (2010) Flexible, magnetic, and electrically conductive graphene/fe3o4 paper and its application for magnetic-controlled switches. J Phys Chem C 114:17465–17471
[36] Ferrand HL, Bolisetty S, Demirörs AF, Libanori R, Studart AR, Mezzenga R (2016) Magnetic assembly of transparent and conducting graphene-based functional composites. Nat Commun 7:12078
[37] Yan H, Wang R, Li Y, Long W (2015) Thermal conductivity of magnetically aligned graphene–polymer composites with fe3o4 -decorated graphene nanosheets. J Electron Mater 44:658–666
[38] Erb RM, Segmehl J, Charilaou M, Löffler JF, Studart AR (2012) Non-linear alignment dynamics in suspensions of platelets under rotating magnetic fields. Soft Matter 8(29):7604–7609
[39] Billaud J, Bouville F, Magrini T, Villevieille C, Studart AR (2016) Magnetically aligned graphite electrodes for high-rate performance Li-ion batteries. Nat Energy 1:16097
[40] Castellano RJ, Akin C, Giraldo G, Kim S, Fornasiero F, Shan JW (2015) Electrokinetics of scalable, electric-field-assisted fabrication of vertically aligned carbon-nanotube/polymer composites. J Appl Phys 117:1942–1945
[41] Wu S, Ladani RB, Zhang J et al (2015) Aligning multilayer graphene flakes with an external electric field to improve multifunctional properties of epoxy nanocomposites. Carbon 94:607–618
[42] Wang Z (2009) Alignment of graphene nanoribbons by an electric field. Carbon 47:3050–3053
[43] Pang H, Chen C, Zhang YC, Ren PG, Yan DX, Li ZM (2011) The effect of electric field, annealing temperature and filler loading on the percolation threshold of polystyrene containing carbon nanotubes and graphene nanosheets. Carbon 49:1980–1988
[44] Li Q, Guo Y, Li W et al (2012) Ultrahigh thermal conductivity of assembled aligned multilayer graphene/epoxy composite. Chem Mate 26:4459–4465
[45] Koo B, Goli P, Sumant AV, Claro PCDS, Rajh T, Johnson CS, Balandin AA, Shevchenko EV (2014) Toward lithium ion batteries with enhanced thermal conductivity. ACS Nano 8:7202–7207
[46] Liang Q, Yao X, Wang W, Liu Y, Wong CP (2011) A three-dimensional vertically aligned functionalized multilayer graphene architecture: an approach for graphene-based thermal interfacial materials. ACS Nano 5:2392–2401
[47] Xia S, Ni M, Zhu T, Zhao Y, Li N (2015) Ultrathin graphene oxide nanosheet membranes with various d-spacing assembled using the pressure-assisted filtration method for removing natural organic matter. Desalination 371:78–87
[48] Liu W, Song N, Wu Y, Gai Y, Zhao Y (2017) Preparation of layer-aligned graphene composite film with enhanced thermal conductivity. Vacuum 138:39–47
[49] Song N, Jiao D, Ding P, Cui S, Tang S, Shi LY (2015) Anisotropic thermally conductive flexible films based on nanofibrillated cellulose and aligned graphene nanosheets. J Mater Chem C 4:305–314
[50] Lin X, Shen X, Zheng Q, Yousefi N, Ye L, Mai YW, Kim JK (2012) Fabrication of highly-aligned, conductive, and strong graphene papers using ultralarge graphene oxide sheets. ACS Nano 6:10708–10719
[51] Park S, Mohanty N, Suk JW et al (2010) Biocompatible, robust free-standing paper composed of a tween/graphene composite. Adv Mater 22:1736–1740
[52] Zhang YF, Ren YJ, Bai SL (2018) Vertically aligned graphene film/epoxy composites as heat dissipating materials. Int J Heat Mass Tran 118(18):510–517
[53] Zhang J, Xu X, Yao C, Li L (2016) Facile fabrication of an organic semiconductor/graphene microribbon heterojunction by self-assembly. RSC Adv 6:52878–52883
[54] Zhao L, Zhang H, Kim NH et al (2016) Preparation of graphene oxide/polyethyleneimine layer-by-layer

assembled film for enhanced hydrogen barrier property. Compos Part B Eng 92:252–258

[55] Zhang B, Cui T (2011) An ultrasensitive and low-cost graphene sensor based on layer-by-layer nano self-assembly. Appl Phys Lett 98:073116

[56] Hong JY, Shin KY, Kwon OS, Kang H, Jang J (2011) A strategy for fabricating single layer graphene sheets based on a layer-by-layer self-assembly. Chem Commun 47:7182–7184

[57] Pu J, Mo Y, Wan S, Wang L (2013) Fabrication of novel graphene-fullerene hybrid lubricating films based on self-assembly for mems applications. Chem Commun 50:469–471

[58] Tang J, Yang J, Zhou L, Xie J, Chen G, Zhou X (2014) Layer-by-layer self-assembly of a sandwich-like graphene wrapped snox@graphene composite as an anode material for lithium ion batteries. J Mater Chem A 2:6292–6295

[59] Zhao X, Zhang Q, Hao Y, Li Y, Fang Y, Chen D (2010) Alternate multilayer films of poly(vinyl alcohol) and exfoliated graphene oxide fabricated via a facial layer-by-layer assembly. Macromolecules 43:9411–9416

[60] Zhang D, Tong J, Xia B (2014) Humidity-sensing properties of chemically reduced graphene oxide/polymer nanocomposite film sensor based on layer-by-layer nano self-assembly. Sens Actuator B Chem 197:66–72

[61] Kirschner J, Wang Z, Eigler S, Steinrück HP, Jäger CM, Clark T, Hirsch A, Halik M (2014) Driving forces for the self-assembly of graphene oxide on organic monolayers. Nanoscale 6:11344–11350

[62] Li Y, Yang J, Zhou Y, Zhao N, Zeng W, Wang W (2016) Fabrication of gold nanoparticles/graphene oxide films with surface-enhanced raman scattering activity by a simple electrostatic self-assembly method. Colloid Surf A 512:93–100

[63] Zhang D, Liu J, Xia B (2016) Layer-by-layer self-assembly of zinc oxide/graphene oxide hybrid toward ultrasensitive humidity sensing. IEEE Electron Device Lett 37:916–919

[64] Chettri P, Vendamani VS, Tripathi A, Pathak AP, Tiwari A (2016) Self-assembly of functionalised graphene nanostructures by one step reduction of graphene oxide using aqueous extract of artemisia vulgaris. Appl Surf Sci 362:221–229

[65] Yu S, Li N, Higgins D et al (2014) Self-assembled reduced graphene oxide/polyacrylamide conductive composite films. ACS Appl Mater Interfaces 6:19783

[66] Yao Y, Ma W (2014) Self-assembly of polyelectrolytic/graphene oxide multilayer thin films on quartz crystal microbalance for humidity detection. IEEE Sens J 14:4078–4084

[67] Lee KH, Hong JH, Kwak SJ, Min P, Son JG (2015) Spin self-assembly of highly ordered multilayers of graphene-oxide sheets for improving oxygen barrier performance of polyolefin films. Carbon 83:40–47

[68] Tang L, Li X, Du D, He C (2012) Fabrication of multilayer films from regenerated cellulose and graphene oxide through layer-by-layer assembly. Prog Nat Sci 22:341–346

[69] Zhang D, Tong J, Xia B, Xue Q (2014) Ultrahigh performance humidity sensor based on layer-by-layer self-assembly of graphene oxide/polyelectrolyte nanocomposite film. Sens Actuator B Chem 203:263–270

[70] Qi W, Xue Z, Yuan W, Wang H (2013) Layer-by-layer assembled graphene oxide composite films for enhanced mechanical properties and fibroblast cell affinity. Mater Chem B 2:325–331

[71] Yang L, Niu T, Zhang H, Xu W, Zou M, Xu L et al (2017) Self-assembly of suspended graphene wrinkles with high pre-tension and elastic property. 2D Mater 4:041001

[72] Peng L, Xu Z, Liu Z, Guo Y, Li P, Gao C (2017) Ultrahigh thermal conductive yet superflexible graphene films. Adv Mater 29:1700589

[73] Zhang M, Wang Y, Huang L, Xu Z, Li C, Shi G (2015) Multifunctional pristine chemically modified graphene films as strong as stainless steel. Adv Mater 27:6708

[74] Ye X, Zhu Y, Tang Z, Wan Z, Jia C (2017) In-situ chemical reduction produced graphene paper for flexible supercapacitors with impressive capacitive performance. J Power Sources 360:48–58

[75] Bae S, Kim H, Lee Y et al (2010) Roll-to-roll production of 30-inch graphene films for transparent electrodes. Nat Nanotechnol 5:574–578

[76] Schwierz F (2010) Graphene for electronic applications: transistors and more. In: Bipolar/bicmos circuits and technology meeting. IEEE. https://doi.org/10.1109/bipol.2010.5668069

[77] Malekpour H, Chang KH, Chen JC, Lu CY, Nika DL, Novoselov KS, Balandin AA (2014) Thermal conductivity of graphene laminate. Nano Lett 14:5155–5161

[78] Lv W, Xia Z, Wu S et al (2011) Conductive graphene-based macroscopic membrane self-assembled at a liquid–air interface. J Mater Chem 21:3359–3364

[79] Kim T, Kim H, Kwon SW et al (2012) Large-scale graphene micropatterns via self-assembly-mediated process for flexible device application. Nano Lett 12:743–748

[80] Wang F, Mao J (2018) The self-aligning behaviour of graphene nanosheets in the styrene butadiene rubber by controlling curing temperature. Fuller Nanotub Carbon Nanostruct 26:61–68

[81] Fan P, Wang L, Yang J, Chen F, Zhong M (2012) Graphene/poly(vinylidene fluoride) composites with high dielectric

constant and low percolation threshold. Nanotechnology 23:365702
[82] Sun H, Xu Z, Gao C (2013) Multifunctional, ultra-flyweight, synergistically assembled carbon aerogels. Adv Mater 25:2554–2560
[83] Bai H, Li C, Wang X, Shi G (2011) On the gelation of graphene oxide. J Phys Chem C 115:5545–5551
[84] Estevez L, Kelarakis A, Gong Q, Da'as EH, Giannelis EP (2011) Multifunctional graphene/platinum/nafion hybrids via ice templating. J Am Chem Soc 133:6122–6125
[85] Deville S (2010) Freeze-casting of porous ceramics: a review of current achievements and issues. Adv Eng Mater 10:155–169
[86] Li WL, Lu K, Walz JY (2012) Freeze casting of porous materials: review of critical factors in microstructure evolution. Int Mater Rev 57:37–60
[87] Qiu L, Liu JZ, Chang SL, Wu Y, Li D (2012) Biomimetic superelastic graphene-based cellular monoliths. Nat Commun 3:1241
[88] Xu Z, Zhang Y, Li P, Gao C (2012) Strong, conductive, lightweight, neat graphene aerogel fibers with aligned pores. ACS Nano 6:7103–7113
[89] Wang Z, Shen X, Han NM, Liu X, Wu Y, Ye W, Kim JK (2016) Ultralow electrical percolation in graphene aerogel/epoxy composites. Chem Mater 28:6731–6741
[90] Li XH, Li X, Liao KN, Min P, Liu T, Dasari A, Yu ZZ (2016) Thermally annealed anisotropic graphene aerogels and their electrically conductive epoxy composites with excellent electromagnetic interference shielding efficiencies. ACS Appl Mater Interfaces 8:33230–33239
[91] Vickery JL, Patil AJ, Mann S (2010) Fabrication of graphene–polymer nanocomposites with higher-order three-dimensional architectures. Adv Mater 21:2180–2184
[92] Wang Z, Han NM, Wu Y, Liu X, Shen X, Zheng Q, Kim JK (2017) Ultrahigh dielectric constant and low loss of highly-aligned graphene aerogel/poly(vinyl alcohol) composites with insulating barriers. Carbon 123:385–394
[93] Zhou X, Yin YX, Cao AM, Wan LJ, Guo YG (2012) Efficient 3d conducting networks built by graphene sheets and carbon nanoparticles for high-performance silicon anode. ACS Appl Mater Inter 4:2824–2828
[94] Zhang Z, Lee CS, Zhang W (2017) Vertically aligned graphene nanosheet arrays: synthesis, properties and applications in electrochemical energy conversion and storage. Adv Energy Mater 7:1700678
[95] Xiong DB, Cao M, Guo Q, Tan Z, Fan G, Li Z, Zhang D (2015) Graphene-and-copper artificial nacre fabricated by a preform impregnation process: bioinspired strategy for strengthening-toughening of metal matrix composite. ACS Nano 9:6934–6943
[96] Chu C, Wang XH, Wang F et al (2018) Largely enhanced thermal conductivity of graphene/copper composites with highly aligned graphene network. Carbon 127:102–112
[97] Chu K, Wang F, Wang XH, Huang DJ (2018) Anisotropic mechanical properties of graphene/copper composites with aligned graphene. Mater Sci Eng A 713:269–277
[98] Chu K, Wang XH, Li YB et al (2018) Thermal properties of graphene/metal composites with aligned graphene. Mater Des 140:85–94
[99] Cao M, Xiong DB, Tan Z et al (2017) Aligning graphene in bulk copper: nacre-inspired nanolaminated architecture coupled with in-situ processing for enhanced mechanical properties and high electrical conductivity. Carbon 117:65–74
[100] Kim Y, Lee J, Yeom MS et al (2013) Strengthening effect of single-atomic-layer graphene in metal-graphene nanolayered composites. Nat Commun 4:2114
[101] Kumar P, Shahzad F, Yu S, Hong SM, Kim YH, Chong MK (2015) Large-area reduced graphene oxide thin film with excellent thermal conductivity and electromagnetic interference shielding effectiveness. Carbon 94:494–500
[102] Alsaleh MH (2016) Electrical and electromagnetic interference shielding characteristics of gnp/uhmwpe composites. J Phys D Appl Phys 49:195302
[103] Kim H, Miura Y, Macosko CW (2010) Graphene/polyurethane nanocomposites for improved gas barrier and electrical conductivity. Chem Mater 22:3441–3450
[104] Yang L, Zhang S, Zheng C, Guo Y, Luan J, Zhi G, Wang G (2014) Design and preparation of graphene/poly(ether ether ketone) composites with excellent electrical conductivity. J Mater Sci 49:2372–2382. https://doi.org/10.1007/s10853-013-7940-2
[105] Ding JN, Fan Y, Zhao CX, Liu YB, Yu CT, Yuan NY (2012) Electrical conductivity of waterborne polyurethane/graphene composites prepared by solution mixing. J Compos Mater 46:747–752
[106] Shah R, Kausar A, Muhammad B, Shah S (2015) Progression from graphene and graphene oxide to high performance polymer-based nanocomposite: a review. Polym Plast Technol Eng 54:173–183
[107] Huang T, Lu R, Su C et al (2012) Chemically modified graphene/polyimide composite films based on utilization of covalent bonding and oriented distribution. ACS Appl Mater Interfaces 4:2699–2708
[108] Gao J, Itkis ME, Yu A, Bekyarova E, Zhao B, Haddon RC (2005) Continuous spinning of a single-walled carbon nanotube-nylon composite fiber. J Am Chem Soc 127:3847–3854
[109] Huang HD, Ren PG, Chen J, Zhang WQ, Ji X, Li ZM (2012) High barrier graphene oxide nanosheet/poly(vinyl

alcohol) nanocomposite films. J Membr Sci 409–410:156–163

[110] Tung VC, Kim J, Cote LJ, Huang JX (2011) Sticky interconnect for solution-processed tandem solar cells. J Am Chem Soc 133(24):9262–9265

[111] Chen F, Ying J, Wang Y, Du S, Liu Z, Huang Q (2016) Effects of graphene content on the microstructure and properties of copper matrix composites. Carbon 96:836–842

[112] Liu P, Zhang X, Jia H, Yin Q, Wang J, Yin B, Xu D (2017) High mechanical properties, thermal conductivity and solvent resistance in graphene oxide/styrene-butadiene rubber nanocomposites by engineering carboxylated acrylonitrile-butadiene rubber. Compos Part B Eng 130:257–266

[113] Höltker G (2013) Enhanced mechanical and gas barrier properties of rubber nanocomposites with surface functionalized graphene oxide at low content. Polymer 54:1930–1937

[114] Xing W, Wu J, Huang G, Li H, Tang M, Fu X (2014) Enhanced mechanical properties of graphene/natural rubber nanocomposites at low content. Polym Int 63(9):1674–1681

[115] Uddin ME, Layek RK, Kim HY, Kim NH, Hui D, Lee JH (2016) Preparation and enhanced mechanical properties of non-covalently-functionalized graphene oxide/cellulose acetate nanocomposites. Compos Part B Eng 90:223–231

[116] Wu Y, Chen L, Li J, Zhou H, Zhao H, Chen J (2017) Understanding the mechanical and tribological properties of solution styrene butadiene rubber composites based on partially graphene oxide. Eur Polym J 89:150–161

[117] Gao X, Yue H, Guo E, Zhang H, Lin X, Yao L, Wang B (2016) Mechanical properties and thermal conductivity of graphene reinforced copper matrix composites. Powder Technol 301:601–607

[118] Li A, Zhang C, Zhang YF, Li A, Zhang C, Zhang YF (2017) Thermal conductivity of graphene-polymer composites: mechanisms, properties, and applications. Polymers 9:437

[119] Balandin AA (2011) Thermal properties of graphene and nanostructured carbon materials. Nat Mater 10:569

[120] Shahil KMF, Balandin AA (2012) Graphene-multilayer graphene nanocomposites as highly efficient thermal interface materials. Nano Lett 12:861–867

[121] Goyal V, Balandin AA (2012) Thermal properties of the hybrid graphene-metal nano-micro-composites: applications in thermal interface materials. Appl Phys Lett 100:073113

[122] Saadah M, Hernandez E, Balandin AA (2017) Thermal management of concentrated multi-junction solar cells with graphene-enhanced thermal interface materials. Appl Sci 7:589

[123] Renteria JD, Ramirez S, Malekpour H, Alonso B, Centeno A, Zurutuza A, Cocemasov AI, Nika DL, Balandin AA (2015) Strongly anisotropic thermal conductivity of free-standing reduced graphene oxide films annealed at high temperature. Adv Funct Mater 25:4664–4672

[124] Ma WS, Li J, Zhao XS (2013) Improving the thermal and mechanical properties of silicone polymer by incorporating functionalized graphene oxide. J Mater Sci 48:5287–5294. https://doi.org/10.1007/s10853-013-7320-y

[125] Chatterjee S, Wang JW, Kuo WS et al (2012) Mechanical reinforcement and thermal conductivity in expanded graphene nanoplatelets reinforced epoxy composites. Chem Phys Lett 531:6–10

[126] Aradhana R, Mohanty S, Nayak SK (2018) Comparison of mechanical, electrical and thermal properties in graphene oxide and reduced graphene oxide filled epoxy nanocomposite adhesives. Polymer 141:109–123

[127] Yang B, Shi Y, Miao JB, Xia R, Su LF, Qian JS, Chen P, Zhang QL, Liu JW (2018) Evaluation of rheological and thermal properties of polyvinylidene fluoride (PVDF)/graphene nanoplatelets (GNP) composites. Polym Test 67:122–135

[128] Zhang W, Zuo H, Zhang X, Wang J, Guo L, Peng X (2018) Preparation of graphene-perfluoroalkoxy composite and thermal and mechanical properties. Polymers 10:700

[129] Huang X, Lin Y, Fang G (2018) Thermal properties of polyvinyl butyral/graphene composites as encapsulation materials for solar cells. Sol Energy 161:187–193

[130] Guo Y, Xu G, Yang X, Ruan K, Ma T, Zhang Q, Gu J, Wu Y, Liu H, Guo Z (2018) Significantly enhanced and precisely modeled thermal conductivity in polyimide nanocomposites with chemically modified graphene via in situ polymerization and electrospinning-hot press technology. J Mater Chem C 6:3004

[131] Saboori A, Pavese M, Badini C, Fino P (2017) A novel approach to enhance the mechanical strength and electrical and thermal conductivity of Cu-GNP nanocomposites. Metall Mater Trans A 49:1–13

[132] Li J, Cui J, Yang J, Li Y, Qiu H, Yang J (2016) Reinforcement of graphene and its derivatives on the anticorrosive properties of waterborne polyurethane coatings. Compos Sci Tech 129:30–37

[133] Okafor PA, Singh-Beemat J, Iroh JO (2015) Thermomechanical and corrosion inhibition properties of graphene/epoxy ester-siloxane-urea hybrid polymer nanocomposites. Prog Org Coat 88:237–244

[134] Hikku GS, Jeyasubramanian K, Venugopal A, Ghosh R (2017) Corrosion resistance behaviour of graphene/

polyvinyl alcohol nanocomposite coating for aluminium-2219 alloy. J Alloy Compd 716:259–269

[135] Liu J, Lei H, Li S, Yu M (2015) Graphene dip coatings: an effective anticorrosion barrier on aluminum. Appl Surf Sci 327:241–245

[136] Chang CH, Huang TC, Peng CW, Yeh TC, Lu HI, Hung WI, Weng CJ, Yang TI, Yeh JM (2012) Novel anticorrosion coatings prepared from polyaniline/graphene composites. Carbon 50:5044–5051

[137] Mahato N, Cho MH (2016) Graphene integrated polyaniline nanostructured composite coating for protecting steels from corrosion: synthesis, characterization, and protection mechanism of the coating material in acidic environment. Constr Build Mater 115:618–633

[138] Luo X, Zhong J, Zhou Q, Du S, Yuan S, Liu Y (2018) Cationic reduced graphene oxide as self-aligned nanofiller in the epoxy nanocomposite coating with excellent anticorrosive performance and its high antibacterial activity. ACS Appl Mater Interfaces 10:18400–18415

[139] Liu J, Yu Q, Yu M, Li S, Zhao K, Xue B, Zu H (2018) Silane modification of titanium dioxide-decorated graphene oxidenanocomposite for enhancing anticorrosion performance of epoxy coatings on AA-2024. J Alloy Compd 744:728–739

[140] Pourhashem S, Vaezi MR, Rashidi A, Bagherzadeh MR (2016) Exploring corrosion protection properties of solvent based epoxy-graphene oxide nanocomposite coatings on mild steel. Corros Sci 115:78–92

[141] Li Y, Wang Q, Wang T, Pan G (2012) Preparation and tribological properties of graphene oxide/nitrile rubber nanocomposites. J Mater Sci 47:730–738. https://doi.org/10.1007/s10853-011-5846-4

[142] Wang F, Mao J (2018) Double layer aligned-graphene nanosheets/styrene-butadiene rubber composites: tribological and mechanical properties. J Appl Polym Sci. https://doi.org/10.1002/app.46939

[143] Wu Y, Chen L, Qin S, Li J, Zhou H, Chen J (2017) Functionalized graphene reinforced rubber composite: mechanical and tribological behavior study. J Appl Polym Sci 134:44970

[144] Chen C, Qiu S, Cui M, Qin S, Yan G, Zhao H, Wang L, Xue Q (2017) Achieving high performance corrosion and wear resistant epoxy coatings via incorporation of noncovalent functionalized graphene. Carbon 114:356–366

[145] Pang W, Ni Z, Wu JL, Zhao Y (2018) Investigation of tribological properties of graphene oxide reinforced ultra-high molecular weight polyethylene under artificial seawater lubricating condition. Appl Surf Sci 434:273–282

[146] Wang W, Huang C, Guo Y, Song Y, Zhang Y, Liu Y, Du W (2015) Application research progress of graphene composites in electromagnetic fields. Eng Plast Appl 43:143–146

[147] Kang J, Kim D, Kim Y, Choi JB, Hong BH, Kim SW (2017) High-performance near-field electromagnetic wave attenuation in ultra-thin and transparent graphene films. 2D Mater 4:025003

[148] Drakakis E, Kymakis E, Tzagkarakis G, Louloudakis D, Katharakis M, Kenanakis G, Suchea M, Tudose V, Koudoumas E (2016) A study of the electromagnetic shielding mechanisms in the GHz frequency range of graphene based composite layers. Appl Surf Sci 398:15–18

[149] Yousefi N, Sun X, Lin X, Shen X, Jia J, Zhang B, Tang B, Chan M, Kim JK (2014) Highly aligned graphene/polymer nanocomposites with excellent dielectric properties for high-performance electromagnetic interference shielding. Adv Mater 26:5480–5487

[150] Song WL, Cao MS, Lu MM, Yang J, Ju HF, Hou ZL, Liu J, Yuan J, Fan L (2013) Alignment of graphene sheets in wax composites for electromagnetic interference shielding improvement. Nanotechnology 24:115708

[151] Zhang HB, Yan Q, Zheng WG, He Z, Yu ZZ (2011) Tough graphene-polymer microcellular foams for electromagnetic interference shielding. ACS Appl Mater Interfaces 3:918–924

[152] Kim JM, Lee Y, Jang MG, Han C, Kim WN (2016) Electrical conductivity and emi shielding effectiveness of polyurethane foam-conductive filler composites. J Appl Polym Sci 134:44373